University of Maribor
Faculty of Energy Technology

Journal of ENERGY TECHNOLOGY

Volume 12 / Issue 3
NOVEMBER 2019
www.fe.um.si/en/jet.html

Journal of ENERGY TECHNOLOGY

VOLUME 12 / Issue 3

Revija Journal of Energy Technology (JET) je indeksirana v bazah INSPEC© in Proquest's Technology Research Database.

The Journal of Energy Technology (JET) is indexed and abstracted in database INSPEC© and Proquest's Technology Research Database.

JOURNAL OF ENERGY TECHNOLOGY

Tehnični urednik / TECHNICAL EDITOR

Sonja Novak

Tehnična podpora / TECHNICAL SUPPORT

Tamara BREČKO BOGOVČIČ

Izhajanje revije / PUBLISHING

Revija izhaja štirikrat letno v nakladi 100 izvodov. Članki so dostopni na spletni strani revije - www.fe.um.si/si/jet.html / The journal is published four times a year. Articles are available at the journal's home page - www.fe.um.si/en/jet.html.

Cena posameznega izvoda revije (brez DDV) / Price per issue (VAT not included in price): 50,00 EUR

Informacije o naročninah / Subscription information: http://www.fe.um.si/en/jet/subscriptions.html

Lektoriranje / LANGUAGE EDITING

Terry T. JACKSON

Oblikovanje in tisk / DESIGN AND PRINT

Fotografika, Boštjan Colarič s.p.

Naslovna fotografija / COVER PHOTOGRAPH

Jurij AVSEC

Oblikovanje znaka revije / JOURNAL AND LOGO DESIGN

Andrej PREDIN

Ustanovni urednik / FOUNDING EDITOR

Andrej PREDIN

Spoštovani bralci revije Journal of energy technology (JET)

Električna energija v Sloveniji danes zadostuje za približno četrtino vseh potreb po energiji. V prihodnjih letih bi se lahko ta delež na račun razvoja električnih avtomobilov, toplotnih črpalk in elektronskih naprav še nekoliko povečal. Velika želja po čim večji proizvodnji električne energije z uporabo obnovljivih virov energije seveda še vedno ostaja. Kakšen bo razvoj v prihodnje, si le stežka predstavljamo, še posebej če spomnimo, da je bila prva žarnica na ogleno nitko izdelana pred 140 leti - izdelal jo je T. A. Edison. Slovenci se lahko pohvalimo, da je le štiri leta po izumu, natančneje 4. aprila 1883, zasvetila prva žarnica v Mariboru. To je bila prva žarnica v tem delu Evrope. Karl Scherbaum, mariborski podjetnik in lastnik parnega mlina, je na Grajskem trgu uvedel električno razsvetljavo s 36 žarnicami v poslovnih prostorih in proizvodnji njegovega podjetja, ter ob vhodu v njegov dom. Leto dni pozneje je bila razsvetljava tudi v Postojnski jami. Seveda sodobne žarnice porabijo bistveno manj energije kot njene predhodnice.

Raziskave po učinkovitem delovanju elektromagnetnih naprav morajo potekati še naprej; v pričujoči številki revije JET lahko preberemo zanimive članke s področja elektromagnetike.

Jurij AVSEC
odgovorni urednik revije JET

Dear Readers of the Journal of Energy Technology (JET)

Electricity in Slovenia currently covers about a quarter of all energy needs. With the development of electric cars, heat pumps, electronic devices, an even greater share is expected in the near future. Of course, there is a great desire to generate electricity through renewable energy sources. It is difficult to imagine what the future will look like, especially if we remember that the first carbon light bulb was manufactured only 140 years ago by Edison. Slovenians can boast that only four years later the first light bulb was turned on in Maribor, on April 4, 1883. It was the first such device in this part of Europe. Karl Scherbaum, a Maribor entrepreneur and owner of a steam mill, introduced electric lighting in the Castle Square with 36 lights in his business premises and in the production of his company, as well as before entering his family's home. A year later, lighting was set up in Postojna Cave. Of course, modern light bulbs consume significantly less energy than their predecessors.

Research on the effective functioning of electromagnetic devices must continue, and in the present issue of JET magazine, we can read interesting articles on related subjects.

Jurij AVSEC
Editor-in-chief of JET

Table of Contents / Kazalo

Journal of Energy Technology

JET Volume 12 (2019) p.p. 11-17
Issue 3, November 2019
Type of article 1.04
www.fe.um.si/en/jet.html

CHALLENGES IN THE EMC STANDARDIZATION OF WIRELESS POWER TRANSFER SYSTEMS

IZZIVI V EMC STANDARDIZACIJI SISTEMOV BREZŽIČNEGA PRENOSA ENERGIJE

Bernd Jaekel [R]

Keywords: electromagnetic emissions, EMC, radiated emissions, wireless power transfer, inductive power transfer

Abstract

Charging of electrical and electronic equipment is currently mostly done via conducted connection to an AC/DC power supply unit. However, trends in technology, also driven by issues of convenience for the user, are moving towards wireless power transfer (WPT). A wireless process, in which most of the power is just used for the transfer of energy, includes the usage of a frequency for the power transfer, hence needing resources in the frequency spectrum. As the frequency spectrum is more or less completely assigned to the usage of radio or other services, such as industrial, scientific or medical (ISM) applications, it turns out to be a relatively complex task to actually decide on which frequencies can be used for WPT technology. This paper describes the challenges in the determination of such frequencies in terms of standardization and presents the related consequences.

Povzetek

Polnjenje električne in elektronske opreme je večinoma izvedeno preko povezave naprave z izmenično ali enosmerno napajalno enoto. Trendi v tehnologiji, ki jih narekuje vprašanje priročnosti za uporabnika, se premikajo proti brezžičnemu prenosu energije (WPT). Brezžični proces, pri katerem se

[R] Corresponding author: Dr Bernd Jaekel, Siemens AG, Digital Industry, D-91058 Erlangen, Germany, E-mail address: bernd.jaekel@siemens.com;

večina moči porabi le za prenos energije, uporablja frekvenco za prenos energije, zato potrebuje vire v frekvenčnem spektru. Odločitev na katerih frekvencah se bo uporabljala tehnologija WPT, se je izkazala za kompleksno, saj je frekvenčni spekter bolj kot ne dodeljen v uporabo radiju in drugim storitvam, kot so recimo ISM frekvenčni pasovi. Članek opisuje izzive v določitvi omenjenih frekvenc v smislu standardizacije in predstavlja s tem povezane posledice.

1 INTRODUCTION

The increasing spread of electrical mobile devices and equipment requires new concepts for charging them in a convenient way. Currently, most devices and equipment are conductively charged by means of an AC/DC power supply. However, an approach that supports wireless charging (i.e., charging without galvanic connection between the device to be charged and the power supply system) has recently been becoming relevant.

This wireless technology is not that entirely new as it has been used for some applications for decades, with the prominent example of induction cooking appliances. The fundamental frequency being used for them is in the range of a few tens of kHz. Though there is the potential of causing interference with radio and broadcast reception or with other systems using those frequency ranges for wireless communication, the number of interference cases has shown to be very limited, as those appliances have to comply with emission limits. These limits were derived a long time ago, based on some unknown investigations and arguments, but the limits have been shown to be sufficient. The main reason for both the relatively low limits and the readiness of manufacturers to have accepted them is a technical one: the stray fields of such a wireless power transfer depend mostly on the air gap between the primary and secondary coils. This air gap is very small in the case of placing pots on an induction cooking surface.

Recently, WPT technology has also been introduced to other types of equipment, for example, the charging of mobile devices. However, the biggest issues are currently connected to a new area related to the prominent and promoted topic of electric vehicles. Most of them are currently charged by means of conductive charging, but charging in a wireless power transfer is expected.

This results in several issues to be considered and solved: as it is not convenient and practical to have different charging systems and requirements for different types and brands of vehicles, the need for standardization arises. In terms of compatibility, this means that there should be an agreement on the topology of the coils involved, and on the frequencies used for the wireless process.

In terms of electromagnetic compatibility (EMC), those issues cause further problems. The wireless charging process needs a system of primary and secondary coils that are separated by a more or less large air gap, with stray fields leaving the coil systems. The transfer power under discussion reaches up to several hundred kW and, consequently, the stray fields represent a potential threat to the immunity of other equipment not involved in the transfer process, and also represent a potential issue for personal safety.

2 FREQUENCIES USED FOR WPT

With regard to selecting a suitable frequency for the wireless process, the fact that nearly all frequencies are assigned to the usage of radio communication or other types of services has to be taken into account. There are a few ISM (industrial/scientific/medical) frequencies identified by the ITU (International Telecommunication Union) for the usage of services with nearly unlimited power, but those frequencies are not suitable for the systems used for electric vehicle charging from a technical point of view.

Therefore, only two possibilities exist: to identify frequencies for which there is only a low probability of interfering with radio services or to use arbitrary frequencies but apply the established limits that were introduced long ago for protecting radio services. As the latter possibility can hardly be followed because of the relatively huge power involved in the power transfer, the first possibility is currently investigated in the standardization groups.

IEC CISPR B is the relevant international standardization committee for this topic; the technical specifications taking into account frequency ranges, limits and measurement procedures are expected to become part of a future edition of the standard CISPR 11. Hence in a certain respect, the following information reflects the discussion and development currently underway in the committee CISPR B (in detail, see the recent IEC publications, *[1]*, *[2]*).

Frequency ranges suitable for WPT charging of electric vehicles are listed in Table 1, together with some information regarding their usage.

Table 1: *Candidate frequency bands considered for wireless power transfer in the frequency range below 150 kHz*

Frequency range (kHz)	**Typical WPT use** [c]
19 to 25	Local WPT via an air gap in cm range, throughput power up to 200 kW – automated in-plant transportation systems, trams and electric buses
36 to 40	Local WPT via an air gap in cm range, throughput power up to 200 kW – automated in-plant transportation systems, trams, and electric buses
55 to 65 [a]	Local WPT via an air gap in cm range, throughput power up to 200 kW – automated in-plant transportation systems, trams and electric buses
79 to 90 [b]	Local WPT via an air gap in cm range, throughput power in the range up to 22 kW – electric personal passenger vehicles (e.g., automobiles) and automated in-plant transportation systems
130 to 135	Local WPT via an air gap in cm range, throughput power up to 90 kW – automated in-plant transportation systems

[a] It should be noted that 60 kHz is used as a standard frequency and time signal service.

[b] Candidate WPT frequency range for global harmonization.
The frequency range of 79 kHz to 90 kHz is being considered for electric vehicles.

[c] The power for WPT systems is given for information only.

3 ASSIGNMENT OF WPT SYSTEMS

The CISPR 11 standard applies to industrial, scientific, and medical electrical equipment operating in the frequency range 0 Hz to 400 GHz and to domestic and similar appliances. WPT systems used for the charging of electric vehicles are assigned to it. With respect to the application of appropriate limits for conducted and radiated disturbances for the various types of equipment, CISPR 11 uses a classification scheme according to which WPT systems are categorized as Group 2 equipment. Such equipment contains all ISM (Industrial/Scientific/Medical) RF (radio frequency) equipment in which radio-frequency energy in the frequency range 9 kHz to 40 GHz is intentionally generated and used or only used locally, in the form of electromagnetic radiation, inductive and/or capacitive coupling, for the treatment of material, for inspection/analysis purposes, or for transfer of electromagnetic energy.

In essence, CISPR 11 already contains disturbance limits for Group 2 equipment, for Class A type equipment intended to be used in the industrial environment as well as for Class B type equipment which is intended for the residential area. Consequently, this standard can already be used for measuring WPT systems, for example, to demonstrate compliance with an international specification.

However, the physical parameters and their future use case could imply that the existing limits might have to be amended in order to take into account the interference situation, which could occur if many WPT systems are installed.

4 LIMITS FOR WPT SYSTEMS

There are more or less three aspects which need to be considered when discussing limits (including appropriate measurement methods) for the WPT systems intended to be used for the charging of electric vehicles.

(1) radiated disturbances in the frequency range below 150 kHz,

(2) disturbances produced by the wireless power port, i.e., the cabling arrangement between the secondary terminal of the power electronics and the primary coil, and

(3) consideration of whether the limits above 150 kHz are appropriate for this kind of equipment, also in the light of the expected spreading of its usage.

To date, limits in the frequency range below 150 kHz have been applied relatively seldom and only for special types of equipment, such as induction cooking appliances. The main reason for not having commonly used limits is because there are only a few types of equipment producing intentional disturbances in that frequency range and that there are not that many radio services that could be disturbed. However, aspect (1) is expected to become more and more important because the use cases connected to WPT are expected to have widespread usage and hence a high number of interference sources.

When discussing limits in the frequency range, a closer look has to be taken to identify the radio services to be protected. The investigations showed that typically time signals use this frequency range. Therefore, in a first step, limits have to be derived in such a way that the reception of time signals should continue without being disturbed. The implementation of this

requirement, together with the fact that WPT systems produce relatively strong electromagnetic fields at their fundamental frequencies, has led to a concept that can be called the "chimney approach". This means that a certain relaxation is allowed only for those frequency bands in which the fundamental WPT frequency is located, and relatively tight limits will be required outside of these bands. Of course, it has to be ensured that the frequency bands actually used for WPT do not clash with frequencies used for time signals, for example.

A proposal for limits for the H-field in the frequency range from 9 kHz to 150 kHz is shown in Fig. 1, *[2]*. It has to be noted that the limits shown apply to Class B WPT systems with rated power between 1 kW and 7.7 kW, and measured at a measurement distance of 10 m. For WPT systems with higher power, the limits in the "chimney frequency bands" are relaxed by 15 dB.

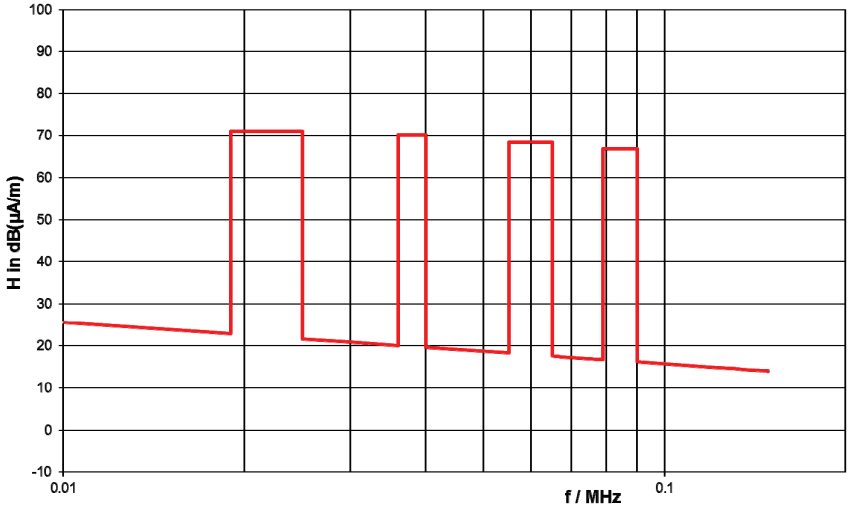

Figure 1: *Radiated limits currently under discussion*

Aspect (2) mentioned above considers the situation that the cable between the output of the power electronics and the coil could be relatively long, thus representing an efficient radiator. Therefore, limits for that interference situation have been discussed. One possibility would be to introduce limits for conducted disturbances on that port. In order to ensure a defined measurement setup, a kind of artificial network would be needed in this circuit. Investigations have shown that this would be very difficult to establish as this circuit is highly sensitive to any parasitic impedances (caused by the artificial network) because this would detune the resonance behaviour of the circuit needed for supplying the coil at discrete frequencies.

An alternative approach would consist of the performance of radiated measurements. There is currently a measurement setup under discussion for E-field measurements in the frequency range from 150 kHz to 30 MHz.

Regarding aspect (3), it should be noted that the current edition of CISPR 11 already specifies limits for the H-field in the frequency range from 150 kHz to 30 MHz. These limits were published a long time ago and apply to Group 2 equipment in general, meaning to equipment

that intentionally produces electromagnetic fields, for example, for the treatment of the material. By default, they apply to WPT systems as well. However, it had been assumed that Group 2 equipment is not used that frequently and, therefore, the limits are relaxed compared to Group 1 equipment: this results from the fact that CISPR limits are derived on a statistical basis and, therefore, equipment with a relatively low number of installations could have relaxed limits compared to that with a high number of installations.

However, the business case for WPT systems expects a wide spreading of their usage; in the ideal case, nearly one system per household when mostly electric vehicles will be used in future. Hence, the statistical basis currently used for the derivation of Group 2 equipment might not be the correct one, and the limits for WPT systems as Group 2 equipment might have to be modified. Such amended limits are currently derived taking into account the interference model and its associated probabilistic factors of the publication CISPR 16-4-4, *[3].*

Fig. 2 shows the limits (Class B, measurement distance 10 m) derived from that interference model. This derivation results in a straight line starting with 15 dBµA/m at 150 kHz and ending with -22 dBµV/m at 30 MHz. However, due to limitations of the achievable signal to noise ratio for frequencies above 6 MHz, the limit line indicated as option 1 is proposed.

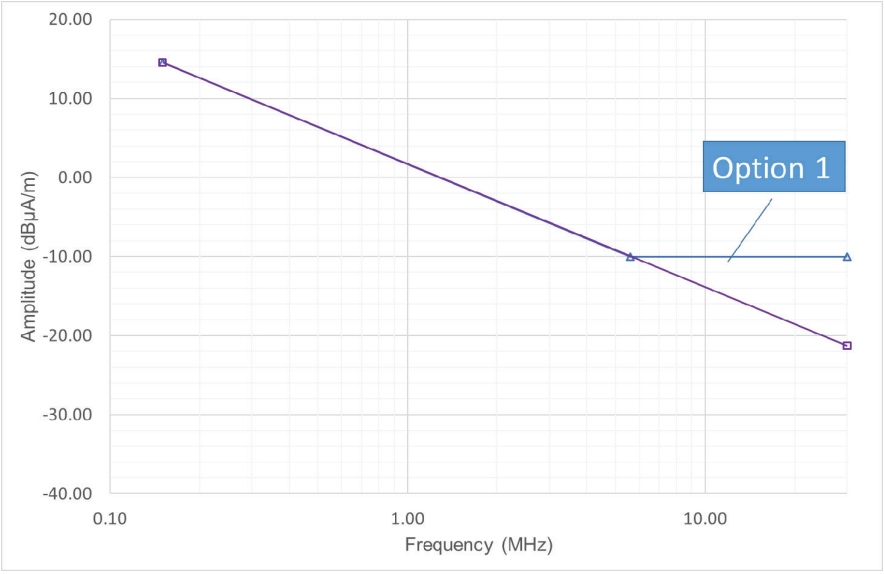

Figure 2: *Proposed H-field limits in the frequency range from 150 kHz to 30 MHz*

5 CONCLUSION

The evolving technology of WPT for charging of electric vehicles requires some attention with respect to the standardization of its emission characteristics. This paper described the challenges associated with it. The ideas and proposals given above are expected to be published in the near future as a document within the IEC CISPR B community for commenting by National Committees.

References

[1] CIS/B/687/CDV, Project CISPR 11/AMD2/FRAG1 ED6: Amendment 2 Fragment 1 to CISPR 11 Ed. 6: Industrial, scientific and medical equipment - Radio-frequency disturbance characteristics - Limits and methods of measurement - Requirements for air-gap wireless power transfer (WPT), Geneva, 2017

[2] CIS/B/710/CD, Project CISPR 11/AMD3/FRAG1 ED6: Amendment 3 Fragment 1 to CISPR 11 Ed. 6: Industrial, scientific and medical equipment - Radio-frequency disturbance characteristics - Limits and methods of measurement - Requirements for air-gap wireless power transfer (WPT), Geneva, 2018

[3] CISPR TR 16-4-4: Specification for radio disturbance and immunity measuring apparatus and methods - Part 4-4: Uncertainties, statistics and limit modelling - Statistics of complaints and a model for the calculation of limits for the protection of radio services calculation of limits for the protection of radio services, Geneva, 2007

Journal of Energy Technology

JET Volume 12 (2019) p.p. 19-29
Issue 3, November 2019
Type of article 1.04
www.fe.um.si/en/jet.html

AN ALTERNATIVE METHOD OF INCREASING THE TRANSMISSION PERFORMANCE OF A CONVENTIONAL 110 kV CABLE LINE

ALTERNATIVNA METODA ZA POVEČANJE PRENOSNIH ZMOGLJIVOSTI KONVENCIONALNE 110 kV LINIJE

Dardan Klimenta[1✉], Dragan Tasić[2], Miroljub Jevtić[1]

Keywords: Ampacity, finite-element method (FEM), hydronic asphalt pavement (HAP), power cable, thermal analysis

Abstract

The purpose of this paper is to show that a significant increase in the ampacity of a 110 kV underground cable line is achievable, if a hydronic asphalt pavement system is applied along the entire line, and if the cable trench is completely filled with high thermal conductivity bedding in order to improve the conduction of heat between the line and the surface of the earth. In such a way, it would be possible to simultaneously collect and then store heat from the sun and cable line. The mutual thermal effects between the 110 kV cable line and the hydronic asphalt pavement, in the presence of solar radiation, wind-driven convection and heat emission along the earth surface, are simulated using FEM-based models for the most unfavourable summer conditions and the most common winter conditions. An adequate experimental background is also provided based on the

✉ Corresponding author: Professor, Dardan Klimenta, Tel.: +381 65 40 666 40, Mailing address: Kneza Miloša St. 7, RS-38220 Kosovska Mitrovica, Serbia, E-mail address: dardan.klimenta@pr.ac.rs

[1] University of Priština in Kosovska Mitrovica, Faculty of Technical Sciences, Kneza Miloša St. 7, RS-38220 Kosovska Mitrovica, Serbia

[2] University of Niš, Faculty of Electronic Engineering, Aleksandra Medvedeva St. 14, RS-18000 Niš, Serbia

existing measurements relevant to the thermal analysis performed. It was found that, compared to the associated base cases, the cable ampacity can be increased up to 92.3% for the most unfavourable summer conditions, and up to 60.3% for the most common winter conditions.

Povzetek

Namen prispevka je prikazati možnost doseganja znatnega povečanja zmogljivosti 110 kV podzemnega vodnika, kadar je vzdolž celotne linije uporabljen hidronični asfalt in v kolikor je kabelski jarek popolnoma zapolnjen z visoko toplotno prevodnim ležiščem, ki izboljša prevodnost toplote med vodnikom in zemeljsko površino. Na tak način bi bilo možno hkrati zbirati in shranjevati toploto sonca in vodnika. Medsebojni toplotni učinki med 110 kV vodnikom in hidroničnim asfaltom ob prisotnosti sončnega sevanja, vetrne konvekcije in oddajanja toplote vzdolž zemeljske površine so v prispevku simulirani z uporabo modelov baziranih na MKE. Za vremenske pogoje so izbrane najbolj neugodne poletne razmere in najpogostejše zimske razmere. Zagotovljeno je ustrezno eksperimentalno ozadje na podlagi obstoječih meritev, ki se nanašajo na opravljeno toplotno analizo. Ugotovljeno je bilo, da je možno na tak način v primerjavi s trenutno izvedbo zmogljivost vodnikov za najbolj neugodne poletne razmere povečati do 92,3 %, za najpogostejše zimske razmere pa do 60,3 %.

1 INTRODUCTION

A hydronic asphalt pavement (HAP) system represents an emerging renewable energy technology, i.e., an innovative method for harvesting energy of the sun, *[1]*. It consists of four main parts, *[2]*: (i) a heat exchanger, i.e. a pavement-solar heat collecting system, (ii) a heat storage system, (iii) a hydronic circulating pump, and (iv) an automatic monitoring system. Fig. 1 provides a detailed depiction of the operating principle of the HAP system, which includes the cooling of pavement in summer, storing the heat in the ground, and the heating of pavement in winter. Since the earth's surface above power cables usually does not freeze during winter, pavement heating using the HAP system is not relevant for that period. Therefore, it is assumed that all collected heat is used for various applications in buildings and process plants or for thermoelectric conversion.

Together with solar energy, the HAP system from Fig. 1 may simultaneously collect some waste heat from power cables if they are installed below the heat exchanger. Collecting both can decrease the surface temperature of the pavement above power cables by approximately 10 °C when compared with the surface temperature of conventional pavement, *[1].* This experimental observation refers to dynamic thermal analysis. This means that the difference corresponding to the steady-state thermal analysis is significantly higher, which makes it possible to use the HAP system in order to increase the cable ampacity under different environmental conditions.

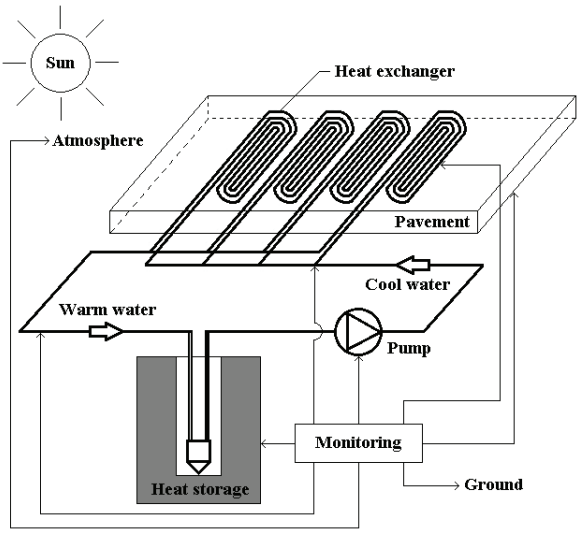

Figure 1: *Operating principle of the HAP system [1,2]*

This paper considers the possibility of increasing the ampacity of the 110 kV underground cable line by an application of the HAP system, under the most unfavourable summer conditions and the most common winter conditions. It is assumed that the HAP system is applied along the entire cable line and that the cable trench is completely filled with one of four different bedding materials with high thermal conductivities. FEM-based models in which the cable beddings have a standard size of 1.2 m × 0.65 m are used as the base cases for the summer and winter periods. Finally, the steady-state thermal analysis reached a number of interesting conclusions.

2 FEM-BASED STEADY-STATE THERMAL MODELS

Fig. 2 illustrates a cross-sectional view of the experimental apparatus that was used in *[1]* for testing HAP system performance. The experiment is relevant for the validation of the model proposed herein. According to *[1]*, the experiment was conducted with the following environmental conditions and material properties:

(i) temperature of the air contacting the pavement surface T_a=32.93 °C;

(ii) heat transfer coefficient due to wind-driven convection h=6 W/(m^2·K);

(iii) solar irradiance incident on the pavement surface $Q_{S,s}$=800 W/m^2;

(iv) solar absorptivity and thermal emissivity of the pavement surface α=0.90625 and ε=0.9, respectively;

(v) water temperature at inlets of the heat collecting pipes $T_{w,i}$=23.2 °C;

(vi) water temperature at outlets of the heat collecting pipes $T_{w,o}$=28.2 °C;

(vii) water velocity in the heat collecting pipes v_w=0.06 m/s or v_w=1 l/min;

(viii) thermal conductivity of the water flowing through the pipe indicated by a white circle in Fig. 2 k=0.61331 W/(m·K) – at T_w=($T_{w,i}$+$T_{w,o}$)/2=25.7 °C;

(ix) thermal conductivity of the still water in the pipes indicated by grey circles in Fig. 2 k=0.64399 W/(m·K) – at 50 °C;

(x) thermal conductivity of the copper pipe k=385 W/(m·K), and

(xi) thermal conductivity of the limestone asphalt mixture/pavement k=1.583 W/(m·K).

The inner and outer diameters of the copper pipes (i.e., heat collecting pipes) are equal to $d_{p,i}$=0.019 m and $d_{p,o}$=0.0222 m, respectively.

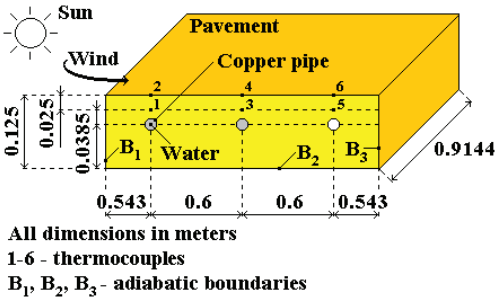

Figure 2: *A cross-sectional view of the experimental apparatus used in [1] for testing HAP system performance (not to scale). Note: In this experiment, water was not flowing through the two pipes indicated by grey circles, while water was flowing through the pipe indicated by a white circle*

Fig. 3a shows the computational domain used for the two base cases, while Fig. 3b shows the computational domain used for the proposed alternative method with a HAP system consisting of seven copper pipes. The first base case relates to the following environmental conditions and material properties, *[3,4]*: (i) T_a=40 °C; (ii) wind velocity v_a=0.22 m/s; (iii) $Q_{S,s}$=1000 W/m^2; (iv) temperature of referent soil of T_{rs}=20 °C; and (v) thermal conductivities of the cable bedding, backfill, native soil and conventional asphalt pavement amounting, respectively, to 1 W/(m·K), 0.4 W/(m·K), 0.4 W/(m·K) and 1.2 W/(m·K). These conditions represent the most unfavourable summer conditions. The second base case relates to the most common winter conditions, namely *[4]*: T_a=5 °C, v_a=0.22 m/s, $Q_{S,s}$=500 W/m^2, T_{rs}=10 °C, and thermal conductivities of the cable bedding, backfill, native soil and conventional asphalt pavement amounting, respectively, to 1 W/(m·K), 0.4 W/(m·K), 0.4 W/(m·K) and 1.2 W/(m·K).

The cables in Fig. 3 are of the type AXLJ 1×1000/190 mm^2 64/110 kV. All the construction elements of these cables are described in *[3]*. For the purposes of simulations using the COMSOL software, these cables are modelled with an equivalent construction composed of the aluminium conductor, cross-linked polyethylene (XLPE) insulation, copper screen, and outer polyethylene (PE) sheath with outer radii 19.2 mm, 35.65 mm, 38.35 mm and 42.15 mm, respectively, as well as with thermal conductivities 239 W/(m·K), 0.286 W/(m·K), 385 W/(m·K) and 0.286 W/(m·K). In addition, it is assumed that dimensions and thermal conductivities of the blocks representing the HAP system in Fig. 3b correspond to the ones from Fig. 2.

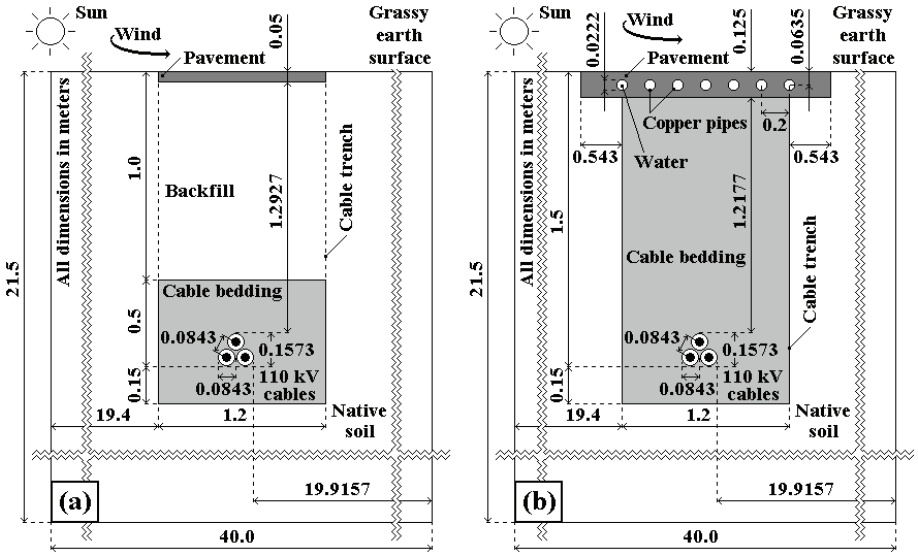

Figure 3: *Presentation of the computational domains for (a) base cases, and (b) proposed method with a HAP system consisting of the same seven copper pipes (not to scale)*

The governing equation for 2D FEM-based modelling of steady-state heat transfer has the following form [3,4]:

$$\frac{\partial}{\partial x}\left(k\frac{\partial T}{\partial x}\right)+\frac{\partial}{\partial y}\left(k\frac{\partial T}{\partial y}\right)+Q_v=0 \tag{2.1}$$

where T is the unknown temperature in K; x, y are the Cartesian spatial coordinates in m; and Q_v is the volume power of heat sources in W/m^3. The thermal conductivities of all bedding materials appearing in the FEM-based models are listed in Table 1. The governing equation is non-linear due to the existence of the radiation boundary conditions.

All the required material and surface properties are constant and selected so that the obtained results are optimistic from the engineering point of view. Accordingly, the values of the thermal and electrical conductivities which correspond respectively to the associated dried-out states (of the cable bedding and the native soil) and the continuously permissible temperature (T_{cp}=90 °C) are taken into account.

Table 1: *Thermal conductivity of all used bedding materials in the dried-out state*

Cable bedding material	k W/(m·K)
Fine aggregate, Serbian standard *[5]*	1
Fine aggregate, US standard *[6]*	1.47
Limestone fine aggregate *[7]*	2.15
Quartzite fine aggregate *[7]*	5.38

The volume power of heat sources Q_v in each 110 kV conductor with a radius of 19.2 mm and a geometric cross-section area of S_c=1158.117·10^{-6} m^2 is

$$Q_v = \frac{R_{ac}(T_{cp})}{S_c} \cdot I^2 \tag{2.2}$$

where $R_{ac}(T_{cp})$=40.91094·10^{-6} Ω/m is the effective conductor resistance to the flow of alternating current per unit length of each 110 kV cable at T_{cp}=90 °C, and I is the ampacity or load current in A. The a.c. resistance takes into account the skin and proximity effects, as well as losses in the metal screen. According to the facts given in *[3,4]*, the volume powers of heat sources in the cable insulation and metal screens of the 110 kV cables are equal to zero.

The adiabatic boundary condition:

$$k \cdot \frac{\partial T}{\partial n} = 0 \tag{2.3}$$

is used to model boundaries surrounding the left-hand, bottom and right-hand sides of the two domains in Fig. 3, where the constant temperature boundary condition:

$$T = T_0(x, y) = T_{rs} + 273.15 \tag{2.4}$$

also needs to be satisfied simultaneously [3,4]. In the Eqn. (2.3) and Eqn. (2.4), n is the length of the normal vector $\vec{n}$ in m, while T and T_0 are the unknown and specified temperatures of the corresponding boundaries in K, respectively.

The heat transfer along the earth and pavement surfaces is represented by a combination of the convection boundary condition:

$$k \cdot \frac{\partial T}{\partial n} = h \cdot (T - T_a) \tag{2.5}$$

and the radiation boundary condition:

$$k \cdot \frac{\partial T}{\partial n} = \varepsilon \cdot \sigma_{SB} \cdot T^4 - \alpha \cdot Q_{S,s} \tag{2.6}$$

where T is the unknown surface temperature of the earth or pavement in K, α=0.6 and ε=0.94 are the solar absorptivity and thermal emissivity for a dry grassy surface, α=0.87 and ε=0.93 are the solar absorptivity and thermal emissivity for the asphalt surfaces in Fig. 3, h=12.654 W/(m^2·K) is the heat transfer coefficient due to convection for a dry grassy surface when v_a=0.22 m/s, h=8 W/(m^2·K) is the heat transfer coefficient due to convection for the asphalt surfaces in Fig. 3 when v_a=0.22 m/s, and σ_{SB}=5.67·10^{-8} W/(m^2·K^4) is the Stefan-Boltzmann constant. More details relating to the boundary conditions (3-6) can be found in *[3,4]*.

The heat transfer between the inner surfaces of the heat collecting pipes and the water flowing through them is represented by the following convection boundary condition:

$$k \cdot \frac{\partial T}{\partial n} = h \cdot (T - T_w) \tag{2.7}$$

where T is the unknown temperature of the corresponding inner boundary in K, which is also higher than T_w=($T_{w,i}$+$T_{w,o}$)/2. Accordingly, the associated Reynolds number Re and heat transfer coefficient h are

$$\mathrm{Re} = \frac{v_w \cdot d_{p,i}}{\nu} < \mathrm{Re}_{cr} = 2300 \tag{2.8}$$

$$h = \frac{3.66 \cdot k}{d_{p,i}} \tag{2.9}$$

where k is the thermal conductivity of water at T_w in W/(m·K), ν is the kinematic viscosity of water at T_w in m^2/s, and Re_{cr} is the critical Reynolds number for smooth pipes. Therefore, the wall temperature of each copper pipe is assumed to be constant. The values of k, ν, Re and h respectively amount to 0.61331 W/(m·K), 8.5776·10^{-7} m^2/s, 1329.04 and 118.14 W/(m^2·K) for T_w=25.7 °C.

3 RESULTS AND OBSERVATIONS

The results obtained by simulating the temperature distribution over the transverse cross-section of the experimental apparatus (Fig. 2) for the known environmental and operating conditions are shown in Figs. 4a and 4b. It is found that the temperature of the surface above the pipes can be decreased by about 12.9 °C with the flowing of water. In comparison with the corresponding experimental result of the dynamic thermal analysis, *[1]*, this temperature is higher by about 2.9 °C and represents the maximum possible value that can be reached for $T_{w,i}$=23.2 °C. According to *[8]*, for $T_{w,i}$=13 °C, the temperature of the surface above the pipes can be decreased by about 18 °C.

However, there are parts of the asphalt pavement surface between the pipes whose temperature is decreased by only 3.7 °C. One way of overcoming this is to increase the number of pipes filled with flowing water. Fig. 4c shows temperature distribution over a domain having seven copper pipes filled with flowing water. The domain and pipes have the same dimensions as those in Fig. 2. In this case, the temperature of the entire surface above the seven copper pipes can be decreased by 14-16 °C. This observation is significant, because it indicates that it is possible to reduce the amount of heat radiated back from the pavement surface.

How the HAP system affects the conductor temperature and load current of the 110 kV cables can best be illustrated by concrete examples of the temperature field distribution over the two computational domains in Fig. 3. Accordingly, Figs. 5a and 5b show the temperature field distributions over the domains in Figs. 3a and 3b, respectively. The temperature distribution in Fig. 5a is obtained for the environmental conditions and material properties corresponding to the first base case (i.e., for the most unfavourable summer conditions). In addition, the result in Fig. 5b is obtained for the same environmental conditions and thermal conductivities of the cable bedding, native soil and limestone asphalt mixture/pavement amounting, respectively, to 5.38 W/(m·K), 0.4 W/(m·K) and 1.583 W/(m·K). In both simulations, the volume powers of heat sources and load currents were Q_v=10250 W/m^3 and I=538.7 A, respectively.

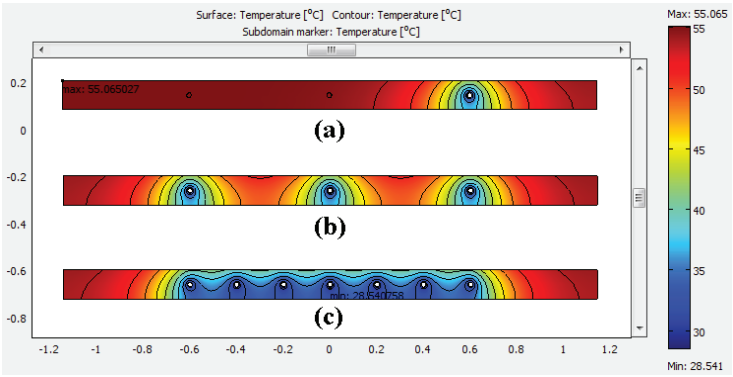

Figure 4: *Temperature distribution over the domain in Fig. 2 for cases when (a) water flows through only one of the three pipes, and (b) water flows through each of the three pipes; (c) temperature distribution over a domain having seven copper pipes filled with flowing water*

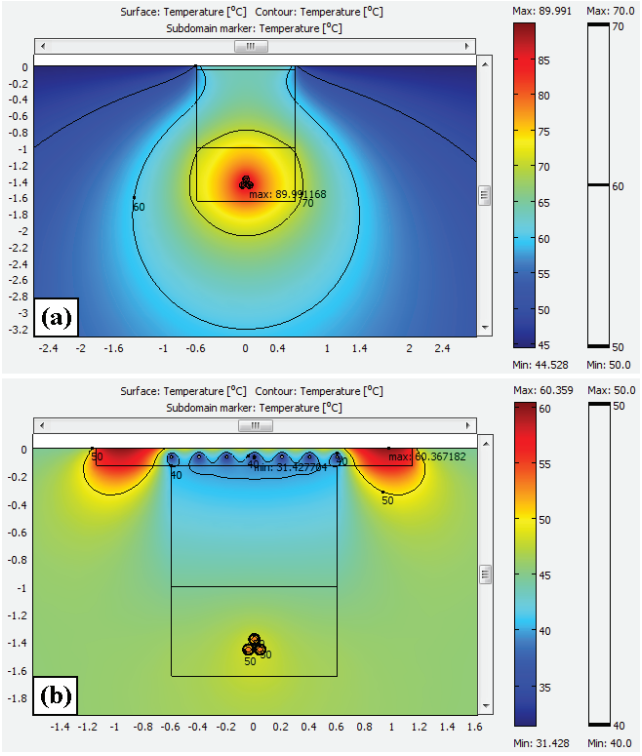

Figure 5: *Temperature distributions over the domains shown in (a) Fig. 3a, and (b) Fig. 3b*

According to Fig. 5, the HAP system in combination with the cable trench that is completely filled with fine quartzite aggregate affects the load current of the 110 kV cable line to a considerable extent. In particular, with the installation of the HAP system, the maximum

system above the 110 kV cable line can be used simultaneously to control the ampacity and to collect heat from the sun and cables.

For the purpose of determining the ampacity of the 110 kV cable line I_{cp}, a sequence of simulations over the two computational domains (in Figs. 3a and 3b) is performed with the thermal conductivities of the selected cable bedding materials (Table 1), for the most unfavourable summer conditions and the most common winter conditions. The values for Q_v are gradually increased from an arbitrary prescribed initial value (e.g., 10 kW/m^3) to its continuously permissible value (corresponding to the temperature T_{cp}=90 °C). The volume powers of heat sources Q_v obtained in this manner are listed in Table 2. Then, these volume powers of heat sources and the Eqn. (2.2) are used to calculate the corresponding cable ampacities (for I=I_{cp}). The ampacities I_{cp} of the considered 110 kV cable line are also listed in Table 2. In order to simplify comparisons between the results, the inlet water temperature is assumed to be constant (at 23.2 °C), regardless of the environmental conditions considered.

Table 2: *Volume powers of heat sources in cable conductors and corresponding ampacities estimated for the computational domains in Figs. 3a and 3b, different cable bedding materials and different environmental conditions*

Cable bedding material	Computational domain	Results obtained for the most unfavourable summer conditions		Results obtained for the most common winter conditions	
k		Q_v	I=I_{cp}	Q_v	I=I_{cp}
W/(m·K)		W/m^3	A	W/m^3	A
1	Fig. 3a	10250	538.7	21185	774.4
1	Fig. 3b	14680	644.6	23735	819.7
1.47	Fig. 3b	18520	724.1	28985	905.8
2.15	Fig. 3b	23195	810.3	35225	998.6
5.38	Fig. 3b	37910	1035.9	54465	1241.7

4 CONCLUSION

The most important conclusions that can be drawn from the presented results are:

- If the conventional asphalt pavement above the 110 kV cable line is changed with the HAP system, combined with the cable trench that is completely filled with the high thermal conductivity bedding, then the corresponding ampacity can be increased up to 497.2 A for the most unfavourable summer conditions and up to 467.3 A for the most common winter conditions.
- HAP systems can be used to control the thermal environment of underground cable lines in order to increase their ampacities.
- The proposed innovative method is new, it can be easily implemented within current practices, and it would result in significant financial and engineering benefits.

Acknowledgements

This paper was based on research conducted within the project TR33046 funded by the Ministry of Education, Science, and Technological Development of the Republic of Serbia.

References

[1] **R.B. Mallick, B.-L. Chen, S. Bhowmick**: *Harvesting heat energy from asphalt pavements: development of and comparison between numerical models and experiment*, International Journal of Sustainable Engineering, Vol. 5, Issue 2, pp. 159-169, 2012

[2] **Z. Zhou, X. Wang, X. Zhang, G. Chen, J. Zuo, S. Pullen**: *Effectiveness of pavement-solar energy system – An experimental study*, Applied Energy, Vol. 138, pp. 1-10, 2015

[3] **D. Klimenta, B. Perović, J. Klimenta, M. Jevtić, M. Milovanović, I. Krstić**: *Controlling the thermal environment of underground cable lines using the pavement surface radiation properties*, IET Generation, Transmission and Distribution, Vol. 12, Issue 12, pp. 2968–2976, 2018

[4] **D.O. Klimenta, B.D. Perović, J.Lj. Klimenta, M.M. Jevtić, M.J. Milovanović, I.D. Krstić**: Controlling the thermal environment of underground power cables adjacent to heating pipeline using the pavement surface radiation properties, Thermal Science, Vol. 22, Issue 6, pp. 2625–2640, 2018

[5] **D. Klimenta, S. Nikolajević, M. Sredojević**: *Controlling the thermal environment in hot spots of buried power cables*, European Transactions on Electrical Power, Vol. 17, Issue 5, pp. 427–449, 2007

[6] **S.Y. King, N.A. Halfter**: *Underground Power Cables*, 1st edition, Longman, London and New York, 1982

[7] **R.B. Mallick, B.-L. Chen, S. Bhowmick, M.S. Hulen**: *Capturing solar energy from asphalt pavements*, The International ISAP Symposium on Asphalt Pavements and Environment (ISAP 2008), Zurich, Switzerland, August 18-20, 2008

[8] **D. Klimenta, D. Tasić, M. Jevtić**: *Increasing the ampacity of a 110 kV underground cable line by an application of a hydronic asphalt pavement system*, The 14th International Conference on Applied Electromagnetics - ПЕС 2019, Niš, Serbia, August 26-28, 2019

Nomenclature

Symbol	Symbol meaning
$d_{p,i}$	inner diameter of the heat collecting pipe, in m
$d_{p,o}$	outer diameter of the heat collecting pipe, in m
h	heat transfer coefficient due to convection, in W/(m^2·K)
I	load current, in A
I_{cp}	ampacity, in A

n	length of the normal vector $\vec{n}$, in m
$\vec{n}$	normal vector
$Q_{S,s}$	solar irradiance, in W/m^2
Q_v	volume power of heat sources, in W/m^3
R_{ac}	effective conductor resistance to the flow of alternating current per unit length of each 110 kV cable at T_{cp}=90 °C, in Ω/m
$\mathbf{Re}$	Reynolds number, dimensionless
$\mathbf{Re}_{cr}$	critical Reynolds number, dimensionless
S_c	geometric cross-section area of each 110 kV conductor, in m^2
T	unknown temperature, in K
T_0	specified temperature, in K
T_a	temperature of the air contacting the pavement surface, in K or °C
T_{cp}	continuously permissible temperature, in °C
T_{rs}	temperature of referent soil, in °C
T_w	average temperature of water flowing inside the heat collecting pipe, in K or °C
$T_{w,i}$	inlet water temperature, in K or °C
$T_{w,o}$	outlet water temperature, in K or °C
v_a	wind velocity, in m/s
v_w	water velocity, in m/s or l/min
x, y	Cartesian spatial coordinates, in m
α	solar absorptivity, dimensionless
ε	thermal emissivity, dimensionless
ν	kinematic viscosity of water, in m^2/s
σ_{SB}	Stefan-Boltzmann constant, in W/(m^2·K^4)

Journal of Energy Technology

JET Volume 12 (2019) p.p. 31-41
Issue 3, November 2019
Type of article 1.04
www.fe.um.si/en/jet.html

INFLUENCE OF ROTOR STRUCTURE ON COGGING TORQUE IN A SURFACE-MOUNTED PM-GENERATOR

VPLIV KONSTRUKCIJE ROTORJA NA SAMODRŽNI VRTILNI MOMENT GENERATORJA S POVRŠINSKO NAMEŠČENIMI TRAJNIMI MAGNETI

Greconici Marian[1], Madescu Gheorghe[2], Milosevici Daniela[3], Biriescu Marius[4], Mot Martian[4,✉]

Keywords: cogging torque, electrical machines, FEM analysis, surface-mounted PM generator

Abstract

This paper deals with the analysis of the cogging torque in a surface-mounted permanent magnet generator in order to determine some techniques to minimize or eliminate the cogging torque. The simulation with finite element method (FEM) was carryout. A four-pole surface-mounted PM generator is investigated in the paper using FEM. The paper analyses the possibilities to reduce this type of torque by producing some asymmetry in the rotor structure. Two types of asymmetry were analysed: the PM pole arc with different widths, and the shifting of the PM. The numerical results obtained in the asymmetrical cases with symmetrical ones were compared and discussed. Finally, some conclusions are highlighted regarding the simulated results.

✉ Corresponding author: Lecturer dr. ing, Moţ Marţian Tel.: +40-256-40-3454, Mailing address: Timişoara, România, B.dul V. Pârvan nr.2, E-mail address: martian.mot@upt.ro

[1] Politehnica University of Timişoara, Fundamentals of Physics for Engineers Department, Timişoara, Romania, B.dul V. Pârvan nr.2.

[2] Romanian Academy – Timişoara Branch, Timişoara, Romania, B.dul M. Viteazul nr. 24

[3] Faculty of Technical Sciences Cacak, Svetog Save 65, 32102 Cacak, Serbia

[4] Politehnica University of Timişoara, Electrical Engineering Department, Timişoara, Romania, B.dul V. Pârvan nr.2.

Povzetek

Članek obravnava analizo samodržnega vrtilnega momenta generatorja s površinsko nameščenimi trajnimi magneti z namenom določitve konstrukcijskih izboljšav oz. metod za zmanjšanje tovrstnega vrtilnega momenta. Obravnavan je štiri polni generator s površinsko nameščenimi trajnimi magneti pri čemer je analiza izvedena z uporabo metode končnih elementov (MKE). V prispevku so analizirane možnosti za zmanjšanje samodržnega vrtilnega momenta z uvedbo asimetrije na rotorju. Analizirana sta dva tipa asimetrije: spremenjena dolžina obodnega loka trajnih magnetov in zamik trajnih magnetov. Pridobljeni numerični rezultati za asimetrične primere so primerjani z simetričnimi. V zaključku sledi razprava v zvezi s pridobljenimi rezultati numeričnih simulacij.

1 INTRODUCTION

The permanent magnet (PM) generator has many attractive characteristics, such as high efficiency and high torque/power density. Consequently, the use of PM machines has increased significantly in the previous two decades in different industrial applications, mainly due to the diminishing cost of the PMs. The absence of excitation currents and the high power factor make the PM machine a winning solution in many cases. That is why many papers deal with the design and optimization of such electrical machines using analytical and numerical methods, *[1-9]*.

The air gap magnetic field density provides much information about estimating motor performance. Moreover, this magnetic field, as an analytical solution, also allows the calculation of some effects, such as cogging torque, ripple torque, back-EMF shape, etc., *[7, 10, 11, 12].*

Paper *[13]* compares five analytical models for predicting the cogging torque in surface-mounted permanent magnet machines.

The cogging torque is normally generated due to the presence of stator slots and results from the interaction between the permanent magnet MMF harmonics and the air gap permeance harmonics due to slotting.

Some design parameters have a great influence on the cogging torque. In *[14]*, the authors have introduced a factor that indicates the “goodness” of a slot and pole number combination with regard to cogging torque.

There are several methods to reduce cogging torque, which may be adopted for rotor structure in surface-mounted PM motors, *[15]*: skewing of the stator slots (or of the PMs), notches in the stator teeth, the width of the PM pole arc, PM pole arc with different widths, shifting of the PMs.

In the present paper, the last two techniques to reduce the cogging torque are analysed and compared using an FEM method.

Some conclusions and discussions are made about these calculated results.

2 GENERATOR TOPOLOGY

A simple four-pole surface-mounted PM generator with the topology illustrated in Figure 1 was used for FEM analysis of cogging torque.

The stator has a classical three-phase winding, star connected, with an integer number of slots per pole per phase (q=3) and single layer: six coil series connected per phase with 42 turns per coil. The cross-section area of conductor: 1.1 mm^2.

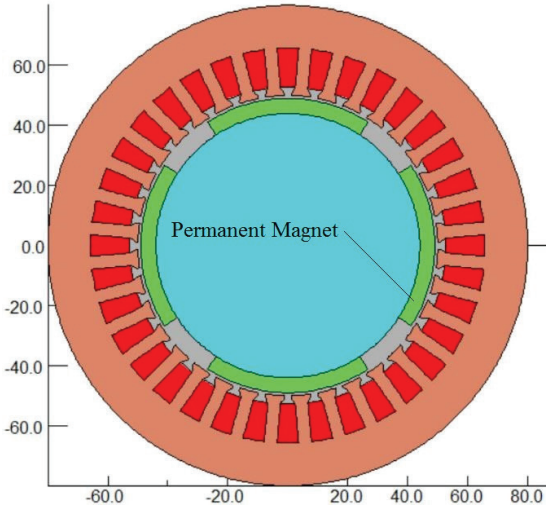

Figure 1: *Cross-section of synchronous surface-mounted PM generator*

The permanent magnets on the rotor surface are mounted. The main specifications of the generator are: power (4 kW); phase number (3); poles number (4); stator slots number (36); stator inner diameter (100 mm); stator length (120 mm); stator outer diameter (160 mm); air-gap thickness (1 mm); permanent magnet thickness (5 mm); Permanent magnet material (NdFeB).

Figure 2 introduces two parameters that are used in the analysis: the width of the PM pole arc (α_m) and the relative position of the magnets (α_{AB}) in the cases of the unsymmetrical arrangement in which the relative positions are different by 90°.

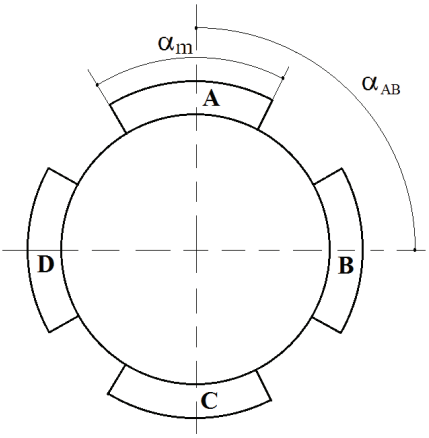

Figure 2: *The width (α_m) and the relative position (α_{AM}) of the magnets*

3 COGGING TORQUE ANALYSIS

The finite element method (OPERA13-Vector Field-software) was used to analyse the cogging torque of a surface-mounted PM generator. Some aspects of these results are presented and discussed.

3.1 Symmetrical rotor structure

In this case, the width of the PM pole arc (α_m) is the same for all the poles (A, B, C, D – Figure 2). Also, the relative position of the magnets present a symmetry, which means α_{AB}= α_{BC}= α_{CD}= α_{DA}=90° (mechanical degree).

In these conditions, Figure 3 shows the air-gap flux density distribution due only to rotor magnets.

The flux density in Figure 3 is provided only by PM with the rotor at standstill (without stator current). It is interesting to note here the same flux density distribution is obtained irrespective of the material placed in the spaces between the PM poles (soft-iron or air). In zone *N* (Figure 3), corresponding to the q-axis, the flux density is zero.

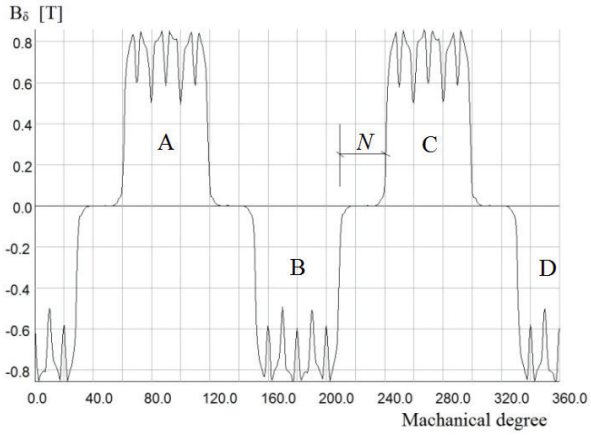

Figure 3: *Air-gap flux density distribution due to rotor magnets*

This air-gap flux density from Figure 3 generates the so-called "cogging torque" component part of the total developed torque. This torque component is due to the presence of stator slots, so that it is zero in slot-less structure. The following expression can be used to calculate this component, *[16]*:

$$T_{cog} = \frac{LR_C^2}{\mu_0}\int_{-\pi}^{\pi}\left(B_{r,PM}\cdot B_{\theta,PM}\right)\cdot \mathrm{d}\theta \tag{3.1}$$

where integration surface is a cylindrical surface in the air-gap with radius R_c and length L (axial length of the stator), and $B_{r,PM}$ and $B_{\theta,PM}$ are, respectively, the radial and tangential components of the air-gap flux density generated by permanent magnets.
Thus, using FEM (in Figure 4) simulated the cogging torque. Again, the same cogging torque waveform as in Figure 4 is obtained in the case with soft-iron pieces placed between the PM poles. The magnitude of cogging torque is about 4% of the working torque.

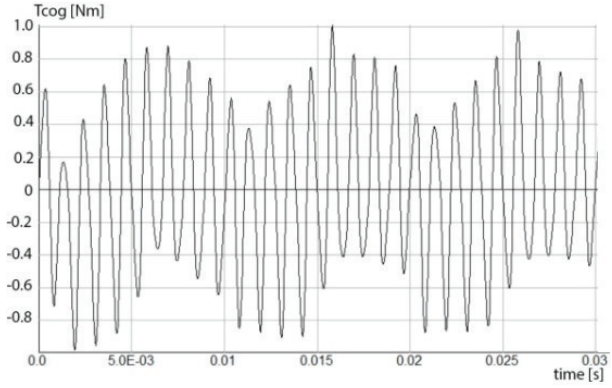

Figure 4: *FEM simulated cogging torque waveform (pole arc of magnets: 66°-mechanical degree).*

The number of periods of the cogging torque waveforms during a rotation (0.04 s) is 36, equal to the number of teeth (36 teeth).

3.2 PM pole arc with different widths

The PM machine can be designed with PMs of different arc widths (α_m). However, all PM rotors of this kind of structure have the same relative position of the magnets. That means: α_{AB}= α_{BC}= α_{CD}= α_{DA}=90° (mechanical degree).

A little asymmetry of the PM widths along the generator airgap can considerably reduce the cogging torque amplitudes. This asymmetry can be arranged in a different manner.

The first type of arrangement is according to Table 1 and includes the FEM simulated cases.

Table 1: *First type of asymmetry*

Case	α_m mechanical degree			
	A	B	C	D
1	70°	66°	70°	66°
2	74°		74°	
3	78°		78°	
4	82°		82°	
5	86°		86°	

Figure 5 and Figure 6 represent the simulated cogging torque for Cases 1 and 2 of Table 1. One can see the influence of the magnets with different pole widths in these figures.

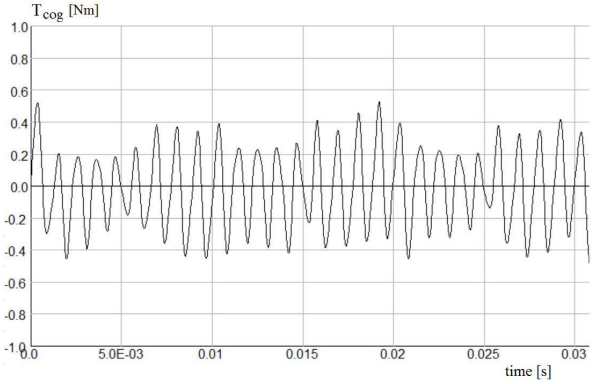

Figure 5: *FEM simulated cogging torque waveform (case1, Table I)*

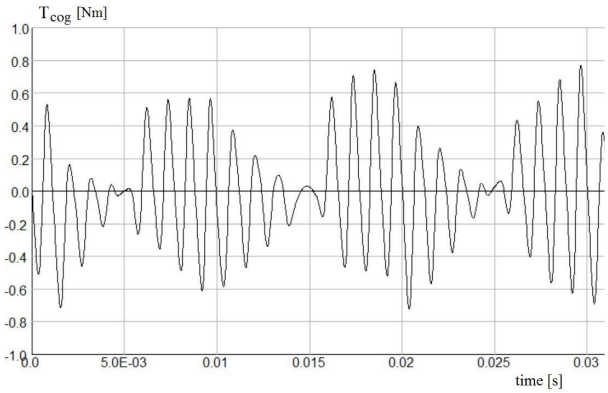

Figure 6: *FEM simulated cogging torque waveform (case2, Table I)*

In Figure 5, it is evident that a small increase in width of the magnets A and C (only 4° mechanical degree) reduces the cogging torque about 50% compared with symmetrical case in Figure 4.

Also, from Figure 6, it can be seen that an additional increase in width of the both A and C magnets does not provide a further decrease of the cogging torque.

Another type of asymmetry is presented in Table 2.

Table 2: *Second type of asymmetry*

Case	α_m mechanical degree			
	A	B	C	D
1	70°	70°	66°	66°
2	74°	74°		
3	78°	78°		
4	82°	82°		
5	86°	86°		

Figure 7 and Figure 8 show the cogging torque simulations in Cases 1 and 2 of Table 2. From this figure it comes out again that a small asymmetry in PM pole widths (around 4°) for two PM poles (magnets A and B) can reduce the cogging torque by 45% compared with the symmetrical case.

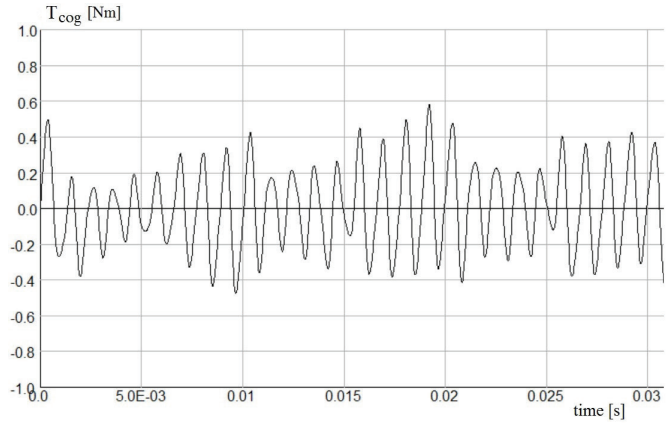

Figure 7: *FEM simulated cogging torque waveform (case1, Table II)*

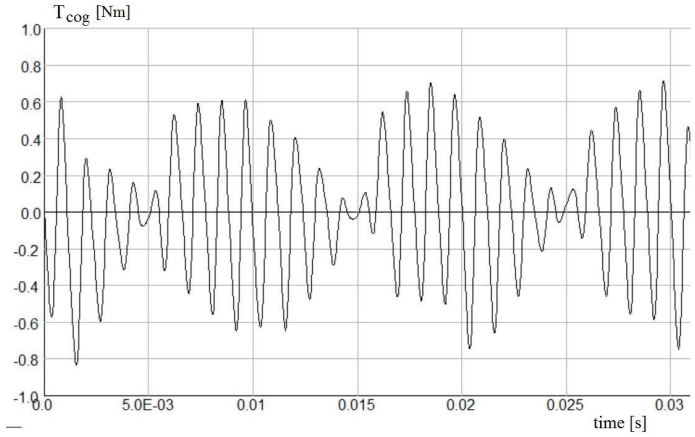

Figure 8: *FEM simulated cogging torque waveform (case2, Table II)*

Consequently, this effect is obtained with a little increase of two PM poles arc (anyone of them), as can be seen in Figure 5 compared with Figure 7.

3.3 Shifting of the PM

The PM generator can be also designed with the same pole arc widths (α_m) and different relative position of the magnets along the airgap. Table 3 includes five cases of this asymmetry type analysed with the FEM method.

Table 3: *Third type of asymmetry*

Case	Pole arc width (α_m)				Position of the magnets			
	A	B	C	D	α_{AB}	α_{BC}	α_{CD}	α_{DA}
1	68	68	68	68	88	92	88	92
2	70	70	70	70	86	94	86	94
3	72	72	72	72	84	96	84	96
4	74	74	74	74	82	98	82	98
5	76	76	76	76	80	100	80	100

Figure 9 shows the simulated cogging torque in Case 1 of Table III. A small asymmetry by shifting of the PM by 2° produces a decrease of the cogging torque by 52% compared with the symmetrical case. A greater shifting in the PM poles distribution along the airgap cannot provide further a smaller cogging torque.

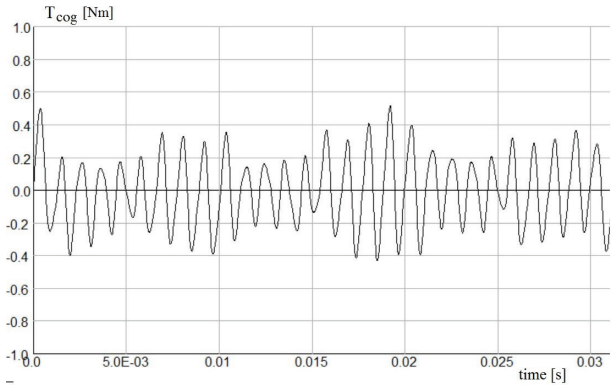

Figure 9: *FEM simulated cogging torque waveform (case1, Table III)*

4 CONCLUSIONS

A four-pole surface-mounted PM generator is investigated in the paper, using FEM. Two methods for minimizing the cogging torque have been analysed. The simulated results show that a small asymmetry in PM pole arc between 4-5% for half of the number of PM poles (anyone of them) is enough to reduce the cogging torque by around 50%. Furthermore, a small asymmetry by shifting of the PM by 2° (mechanical degree) can produce a decrease of the cogging torque by 48%-53%. These two techniques for reducing the cogging torque in a surface-mounted PM generator a very simple and easy to apply.

References

[1] Yao Duan, D. M. Ionel, "A review of recent developments in electrical machine design optimization methods with a permanent magnet synchronous motor benchmark study," *IEEE Transactions on Industry Applications*, 2013, Volume: 49, Issue 3, pp. 1268-1275, DOI: 10.1109/TIA.2013.2252597

[2] S. V. A. Simion, L. Livadaru, N.D. Irimia, F. Lazăr, "FEM analysis of a low speed permanent magnet synchronous machine with external rotor for a wind generator," *Proceedings of OPTIM 2012*, 24-26 May 2012, pp. 624-629, DOI: 10.1109/OPTIM.2012.6231940

[3] M. Pinilla, S. Martinez, "Selection of Main Design Variables for Low-Speed Permanent Magnet Machines Devoted to Renewable Energy Conversion," *IEEE Transactions on Energy Conversion* 2011, Volume: 26, Issue: 3, pp. 940-945, DOI: 10.1109/TEC.2011.2157161

[4] R. Missoum, N. Bernard, M.E. Zaim, J. Bonnefous, "Influence of magnetic materials on maximum power limits of permanent-magnet synchronous machines", *Proceedings of ICEM 2006* paper 696, sept. 4-7, 2006, Chania, Greece

[5] Claudia da Silva, Z. Makni, M. Besbes, C. Marchand, A. Razec, R. Carlson, "Eddy Current Losses and Demagnesization in Permanent Magnets", *Proceedings of ICEM 2006* paper 416, sept. 4-7, 2006, Chania, Greece

[6] N. Bianchi, S. Bolognani, P. Frare, "Design criteria for high-efficiency SPM synchronous motors," *IEEE Transactions on Energy Conversion*, Vol. 21, Issue 2, 2006, pp. 396-404

[7] Aimeng Wang, Yihua Jia, W. L. Soong, "Comparison of Five Topologies for an Interior Permanent-Magnet Machine for a Hybrid Electric Vehicle," *IEEE Transactions on Magnetics*, 2011, Vol. 47, Issue 10, pp. 3606-3609, DOI: 10.1109/TMAG.2011.2157097

[8] Surong Huang, M. Aydin, T. A. Lipo, "Torque quality assessment and sizing optimization for surface mounted permanent magnet machines," *Conference Record of the 2001 IEEE Industry Applications Conference*. 36th IAS Annual Meeting (Cat. No.01CH37248), pp. 1603-610 vol.3, DOI: 10.1109/IAS.2001.955749

[9] V. B. Honsinger, "Performance of Polyphase Permanent Magnet Machines," *IEEE Transactions on Power Apparatus and Systems*, 1980, Vol. PAS-99, Issue: 4, pp. 1510-1518, DOI: 10.1109/TPAS.1980.319575

[10] Z.Q. Zhu, D. Howe, "Instantaneous magnetic field distribution in brushless permanent magnet DC motors. III. Effect of stator slotting", *IEEE Transactions on Magnetics*, 1993 Vol.: 29 , Issue: 1, pp: 143 – 151

[11] A.B. Proca, A. Keyhani, A. El-Antably, Wenzhe Lu, Min Dai, "Analytical model for permanent magnet motors with surface mounted magnets", *IEEE Transactions on Energy Conversion*, 2003 Vol.: 18 , Issue: 3, pp. 386 – 391

[12] Z. J. Liu, J. T. Li, "Accurate Prediction of Magnetic Field and Magnetic Forces in Permanent Magnet Motors Using an Analytical Solution", *IEEE Transactions on Energy Conversion*, 2008 Vol. 23, Issue: 3, Pages: 717 – 726

[13] L. J. Wu, Z. Q. Zhu, D. Staton, M. Popescu, D. Hawkins, "Comparison of analytical models for predicting cogging torque in surface-mounted PM machines", *The XIX International Conference on Electrical Machines - ICEM 2010*, Pages: 1 – 6

[14] Z.Q. Zhu, D. Howe, "Influence of design parameters on cogging torque in permanent magnet machines", *IEEE Transactions on Energy Conversion*, 2000, Vol. 15, Issue: 4, Pages: 407 – 412

[15] N. Bianchi, S. Bolognani, "Design techniques for reducing the cogging torque in surface mounted PM motors" *IEEE Transactions on Industry Applications*, 2002, Vol. 38, Issue: 5, pp. 1259–1265

[16] A. Rahideh, M. Mardaneh, T. Korakianitis, "Analytical 2-D Calculations of Torque, Inductance, and Back-EMF for Brushless Slotless Machines with Surface Inset Magnets", *IEEE Transactions on Magnetics*, 2013, Vol. 49, Issue 8, pp. 4873-4884, DOI: 10.1109/TMAG.2013.2242087

Nomenclature

(Symbols)	(Symbol meaning)
r, θ	polar coordinates
R_c	air-gap radius
L	axial length of the stator
$B_{r,PM}$	radial component of the air-gap flux density generated by PM
$B_{\theta,PM}$	tangential component of the air-gap flux density generated by PM
μ_0	vacuum permeability

Journal of Energy Technology

JET Volume 12 (2019) p.p. 43-52
Issue 3, November 2019
Type of article 1.01
www.fe.um.si/en/jet.html

RESPONSE SURFACE METHOD-BASED OPTIMIZATION OF OUTER ROTOR PERMANENT MAGNET SYNCHRONOUS MOTOR

NAČIN OPTIMIZACIJE ZUNANJEGA ROTORJA ZA TRAJNI MAGNETNI SINHRONSKI MOTOR

Vahid Rafiee[1], Jawad Faiz[✉]

Keywords: Response surface surrogate method, outer rotor permanent magnet synchronous motor, sequential quadratic programming optimization

Abstract

The Finite Element Method (FEM) is a prominent analysis approach. Although it is applicable for simulation and optimization of electrical machines, FEM is a very time-consuming technique. One of the approaches to shorten the optimization runtime is the use of surrogate models instead of FEM. In this paper, the design and optimization of an outer rotor permanent magnet synchronous motor for a hybrid vehicle are investigated. Response surface methodology (RSM) with four input variables is integrated with a sequential quadratic programming algorithm for optimization. Before the optimization, the performance of the surrogate model in the prediction of untried points is validated. Finally, the optimal motor is simulated by FEM to verify the results of RSM-based optimization, and the outputs of both models are compared.

✉ Corresponding author: Professor Jawad Faiz, Tel.: +98 21 6111 4223, Mailing address: Center of Excellence on Applied Electromagnetic Systems, School of Electrical and Computer Engineering. College of Engineering, University of Tehran, North Kargar Avenue, Tehran, E-mail address: jfaiz@ut.ac.ir

[1] Center of Excellence on Applied Electromagnetic Systems, School of Electrical and Computer, Engineering. College of Engineering, University of Tehran, North Kargar Ave, Tehran.

Povzetek

Metoda končnih elementov (FEM) je eden boljših pristopov analize. Čeprav je FEM uporabna za simulacijo in optimizacijo električnih strojev, je pa zelo zamudna tehnika. Eden od pristopov za skrajšanje trajanja optimizacije je uporaba nadomestnih modelov namesto FEM. V prispevku je raziskano načrtovanje in optimizacija sinhronskega motorja s trajnim magnetom zunanjega rotorja za hibridno vozilo. Metodologija odzivne površine (RSM) s štirimi vhodnimi spremenljivkami je integrirana z algoritmom zaporednega kvadratnega programiranja za optimizacijo. Pred optimizacijo je bila uspešnost nadomestnega modela pri napovedovanju neizkušenih točk potrjena. Končno FEM simulira optimalni motor, da preveri rezultate optimizacije na osnovi RSM in primerja izhode obeh modelov.

1 INTRODUCTION

The most well-known method for the optimization of an electromagnetic device is the finite element method (FEM). Using this method requires a long runtime. It is highly desirable to reduce the computational time of these optimizations. One of the best approaches to shortening the computation runtime is based on surrogate modelling in which the outputs for any new, untried point are calculated using the surrogate model. Different artificial intelligence methods, including Kriging, radial basis function (RBF), and response surface method, have been used thus far. Kriging and RBF are more complicated than the response surface method and have multiple distance matrix calculations for new untried points. In contrast, RSM gives the closed-form equations of the system, which enables the designer to use any optimization method, including sequential quadratic programming (SQP).

Optimization of a linear actuator using RSM has been reported in *[2]*. In this paper, the objective of the optimization is to minimize the weight with constraints for thrust force and detent force. The design of a slot-less permanent magnet linear synchronous machine (PMLSM) using RSM with three input variables and two responses has been reported in *[4]*. Rotor pole design in a brushless permanent magnet motor has been proposed in *[5]* in which cogging torque is expressed in terms of three structural variables of the rotor and air gap length in RSM surrogate model. The design and optimization of a PM synchronous motor using an RSM surrogate model to increase constant power speed range (CPSR) has been studied in *[6]*, in which the RSM has three input variables, and a genetic algorithm has been used to optimize the RSM equations.

In the present paper, an outer rotor permanent magnet motor with particular application for hybrid vehicles is designed. To shorten the computational time, the equations of RSM surrogate model of the system are proposed. Finally, the closed-form equations of the motor are optimized using a sequential quadratic programming (SQP) algorithm to determine the optimum point. The results of the RSM and FEM are compared.

2 INITIAL DESIGN OF MOTOR

The design and optimization of an outer rotor surface-mounted permanent magnet machine with 12 slots and 10 poles are investigated here. The proposed machine delivers 400 Nm torque at 1200 rpm. To maximize the fill factor, prefabricated winding has been used, *[7]*; thus, the stator has open slots to enable assembling this type of winding. The magnets of the motor are mounted on the surface of the rotor in the air gap.

3 RESPONSE SURFACE SURROGATE MODEL

The best advantage of the RSM surrogate model is its closed-form equation ($y=f(x_1,x_2...,x_n)$). The outputs functions expressed by the inputs for a linear model are as follows [8]:

$$f(x) = \beta_0 + \sum_{i=1}^{k} \beta_i X_i \tag{3.1}$$

and for quadratic models, it is as follows:

$$f(x) = \beta_0 + \sum_{i=1}^{k} \beta_i X_i + \sum_{ii=1}^{k} \beta_i X_{ii}^2 + \sum_{i<j}^{k} \sum \beta_{ij} X_i X_j \tag{3.2}$$

where β_i, β_j and β_{ij} are the coefficients of the polynomial and X_i and X_j are the input variables of the system.

The coefficients β, are calculated as follows:

$$\beta = [X'X]^{-1} X'y \tag{3.3}$$

where X is the matrix of the input variables and y is the corresponding output values for the sampled points.

4 RSM SURROGATE MODEL OF MOTOR

In this paper, the design space consists of four input variables, and the Box-Behnken RSM surrogate model is used to model this design space. The maximum input current (I_{max}), slot height, the width of the bottom of the slot, and the thickness of the magnets are considered as input variables of this surrogate model. Fig. 1 shows the geometry and three structural input variables.

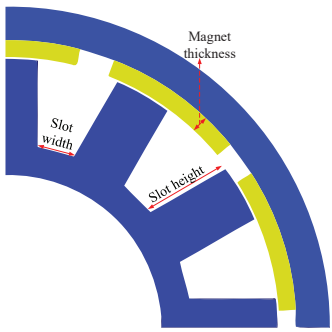

Figure 1: *Geometry and structural variables of the motor*

The range of these variables in the design space has been shown in Table 1. Making a Box-Behnken set of sample points for the surrogate model for a k-dimensional design space requires $2k(k-1)+C_0$ sample point [9], [10]. C_0 is the centre point, and it determines the curvature of the model. Here, four central points are simulated; 28 sample points are generated by Box-Behnken, and the corresponding outputs are calculated using FEM.

Table 1: *Range of input variables*

Input variable	Parameter name	Minimum	Maximum
I_{max}	A	130	160
Slot height	B	20	34
Slot width	C	12	18
Magnet thickness	D	7	12

Table 2 presents the list of simulated points selected by Box Behnken with their corresponding responses. The price, torque, and efficiency of the motor are considered as surrogate model responses. Table 3 shows the analysis of variance (ANOVA) of these responses. In each of the responses, the terms with the p-value higher than 0.1 are insignificant and thus are neglected in the RSM equations. All terms of the equations in efficiency and torque are significant, but in price just six terms are significant, and the others are ignored. The quadratic polynomials of the RSM surrogate model of the system are calculated using Eq. (2) by substituting the simulated matrices of Table 2. The closed-form equations of the price, torque, and efficiency are as follows:

$$\begin{aligned}\mathrm{Price} = 211.1693 + 6.0429B + 3.8953C + 46.74D + 1.0097BC \\ + 0.4897C^2 - 0.5266D^2\end{aligned} \tag{4.1}$$

$$\begin{aligned}Torque = 359.3804 + 36.63A - 12.5602B - 7.6114C + 12.5046D \\ -2.1576AB - 1.2546AC + 2.4269AD - 4.0435BC - 2.5859BD \\ -1.6512CD - 0.7935A^2 - 2.9347B^2 - 1.5774C^2 - 4.7137D^2\end{aligned} \tag{4.2}$$

$$\begin{aligned}Efficiency = 0.9138 - 0.0047A + 0.0129B + 0.0084C + 0.0062D \\ +0.0012AB + 0.0007AC + 0.0005AD - 0.0022BC - 0.0009BD \\ - 0.0005CD - 0.0003A^2 - 0.0035B^2 - 0.0005C^2 - 0.0014D^2\end{aligned} \tag{4.3}$$

The most expensive part of the motor is the magnet, and in Eq. (4), D has the greatest coefficient (46.74). Torque highly depends on the current, and in Eq. (5) the greatest positive coefficient is the coefficient of the current, which is 36.63. As the current and the conduction loss increase, the efficiency decreases. Thus, the current in Eq. (6) has a negative coefficient.

Table 2: *List of sampled points by Box Behnken sampling and corresponding responses*

	A	B	C	D	Price ($)	Torque (Nm)	Efficiency (%)
1	145	34	12	9.5	212.86	354.7	91.63
2	145	27	15	9.5	211.16	359.38	91.38
3	145	20	12	9.5	202.62	371.55	88.58
4	145	34	18	9.5	222.67	330.42	92.91
5	145	20	15	7	157.86	349.38	88.84
6	145	34	15	12	263.35	348.76	92.71
7	130	27	12	9.5	207.76	326	91.01
8	160	20	15	9.5	205.14	406.98	89.09
9	160	27	12	9.5	207.76	402.52	89.94
10	160	34	15	9.5	217.15	377.54	91.9
11	145	27	15	9.5	211.16	359.38	91.38
12	130	20	15	9.5	205.14	329.26	90.32
13	160	27	15	12	257.38	405.42	91.41
14	145	27	12	7	160.49	346.36	0.8967
15	145	34	15	7	169.89	329.25	91.63
16	145	20	15	12	251.37	379.23	90.3
17	145	27	15	9.5	211.16	359.38	91.38
18	145	27	18	7	168.28	334.85	91.45
19	130	34	15	9.5	217.15	308.45	92.64
20	145	27	18	12	261.77	356.33	92.59
21	160	27	15	7	163.89	375	90.04
22	160	27	18	9.5	215.55	385.35	91.74
23	145	20	18	9.5	208.39	363.44	90.77
24	130	27	15	12	257.38	328.21	92.26
25	145	27	15	9.5	211.16	359.38	91.38
26	130	27	15	7	163.89	307.5	91.11
27	145	27	12	12	253.98	374.44	91.03
28	130	27	18	9.5	215.55	313.85	92.50

Table 4 presents the fit statistics of the surrogate model. In this table, C.V% is the coefficient of variance, R^2 is the coefficient of determination. In all responses, the R^2 and adjusted R^2 are close; thus, there is no insignificant variable in the surrogate model, *[8].* Finally, the Adeq precision is the measure of the signal-to-noise ratio. In all responses, the Adeq precision is higher than 4, which shows that the model is desirable and can navigate the design space, *[8]*.

Table 3: *ANOVA for quadratic form of RSM*

Source	p-value		
	Price	**Efficiency**	**Torque**
Model	< 0.0001	< 0.0001	< 0.0001
A	1	< 0.0001	< 0.0001
B	< 0.0001	< 0.0001	< 0.0001
C	< 0.0001	< 0.0001	< 0.0001
D	< 0.0001	< 0.0001	< 0.0001
AB	1	< 0.0001	< 0.0001
AC	1	< 0.0001	0.0004
AD	1	0.0006	< 0.0001
BC	< 0.0001	< 0.0001	< 0.0001
BD	0.6392	< 0.0001	< 0.0001
CD	1	0.0004	< 0.0001
A^2	1	0.0075	0.0029
B^2	0.4254	< 0.0001	< 0.0001
C^2	< 0.0001	0.0002	< 0.0001
D^2	< 0.0001	< 0.0001	< 0.0001

Table 4: *Fit statistics of the RSM surrogate model*

	Price ($)	Torque (Nm)	Efficiency (%)
Mean	211.15	355.09	91.13
C.V%	0.0272	0.1499	0.0264
R^2	1	0.9998	0.9998
Adjusted R^2	1	0.9996	0.9996
Predicted R^2	1	0.999	0.9988
Adeq Prediction	2510.4112	256.2085	242.4228

Fig. 2 presents the actual values calculated by FEM and the predicted values by RSM. This figure shows that there is a good agreement between the predicted and actual values.

5 OPTIMIZATION OF MOTOR

The motor is optimized using the closed-form equations of the RSM surrogate model. The goal

$$\begin{aligned} &\text{Min: Price} \\ &\text{s.t} \quad \text{Torque} > 400 \text{ Nm} \\ &\qquad \text{Efficiency} > 91\% \end{aligned} \tag{5.1}$$

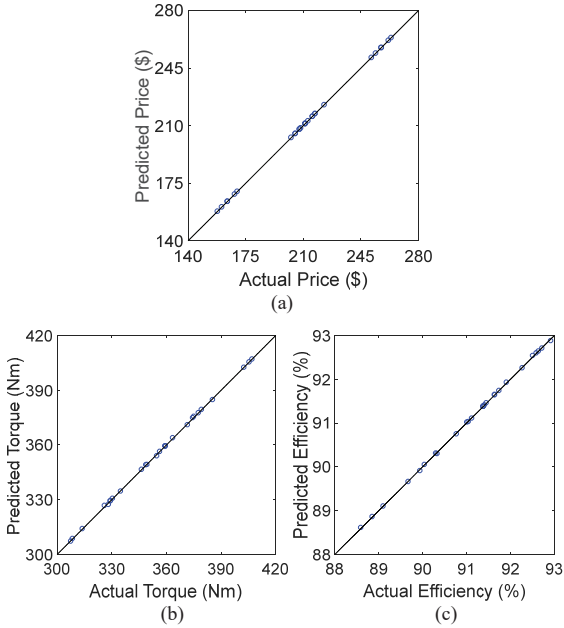

Figure 2: *Predicted versus actual values at sampled points for (a) Price, (b) Torque, (c) Efficiency*

of the optimization is to minimize the price of the motor, considering the following constraints for torque and efficiency.

Sequential quadratic programming (SQP) is applied to optimize the price. The optimization is performed using the RSM equations. The final values of the RSM input parameters at the

Table 5: *Input variables at the optimum point*

Input variable	Parameter symbol	Optimum value
Imax (A)	A	160
Slot height (mm)	B	24.9084
Slot width (mm)	C	16.2131
Thickness of magnet (mm)	D	10.2329

optimum point is presented in Table 5.

After the optimization, the optimal point is simulated by FEM to verify the results of the RSM based optimization. Fig. 3(a) and (b) show the torque and efficiency of the motor at optimum point using FEA in one complete electrical period of the motor, which indicates that the torque and efficiency constraints are satisfied at the optimal point.

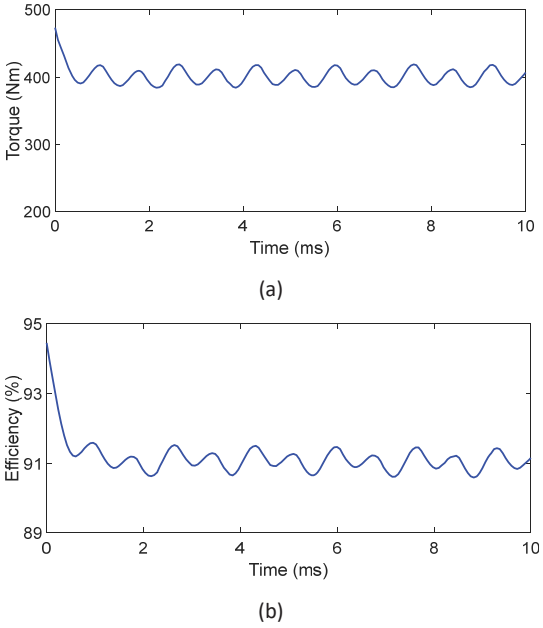

Figure 3: *(a) Torque of optimum motor using FEA (b) efficiency of the optimum motor using FEA*

A full comparison of the RSM and FEM at the optimum point has been presented in Table 6. According to this table, the error of the RSM surrogate model is acceptable; thus, this method can be used instead of FEM in optimizations. For a precise investigation at the optimal point, the field density of the motor at full load is shown in Fig. 4. This figure indicates that there is no saturation in the motor, and a good performance of the motor is guaranteed.

Table 6: *Comparison of RSM and FEA at optimal point*

	RSM	FEA	Error
Price ($)	224.5	224.6	3.87e-04
Torque (Nm)	400	400.4	9.90e-04
Efficiency (%)	91	91.2	2.10e-03

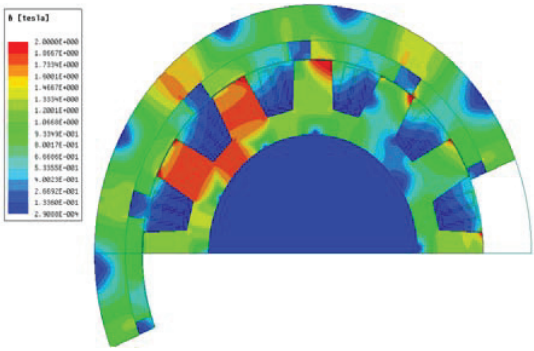

Figure 4: *Magnetic field density distribution of optimal motor at full load operation*

7 CONCLUSION

Generally speaking, the optimization of electromagnetic devices takes a long computation time using FEM. This paper presented an RSM surrogate-based model optimization. All needed outputs of the model were described by closed-form equations in RSM. Having a closed-form set of equations enables the designer to use the best algorithm of optimization, and SQP was used here. Comparison of RSM and FEM results show that there is a good agreement between the RSM surrogate model and FEM. Simulating the motor by FEM at the optimal point verified the results of the RSM based optimization.

8 REFERENCES

[1] **A. Forrester, A. Sobester, and A. Keane:** *Engineering design via surrogate modelling: a practical guide*. John Wiley & Sons, 2008

[2] **H. M. Hasanien, A. S. Abd-Rabou, and S. M. Sakr:** *Design optimization of transverse flux linear motor for weight reduction and performance improvement using response surface methodology and genetic algorithms*, *IEEE Trans. Energy Convers.*, vol. 25, no. 3, pp. 598–605, 2010

[3] **G. Lei, J. Zhu, Y. Guo, C. Liu, and B. Ma:** *A review of design optimization methods for electrical machines*, Energies, vol. 10, no. 12, p. 1962, 2017

[4] **S.-I. Kim, J.-P. Hong, Y.-K. Kim, H. Nam, and H.-I. Cho:** *Optimal design of slotless-type PMLSM considering multiple responses by response surface methodology*, *IEE*E Trans. Magn., vol. 42, no. 4, pp. 1219–1222, 2006

[5] **K.-Y. Hwang, S.-B. Rhee, B.-Y. Yang, and B.-I. Kwon:** *Rotor pole design in spoke-type brushless DC motor by response surface method*, IEEE Trans. Magn., vol. 43, no. 4, pp. 1833–1836, 2007

[6] **L. Jolly, M. A. Jabbar, and L. Qinghua:** *Design optimization of permanent magnet motors using response surface methodology and genetic algorithms*, IEEE Trans. Magn., vol. 41, no. 10, pp. 3928–3930, 2005

[7] **A. M. El-Refaie:** *Fractional-slot concentrated-windings synchronous permanent magnet machines: Opportunities and challenges*, IEEE Trans. Ind. Electron., vol. 57, no. 1, pp. 107–121, 2009

[8] **R. H. Myers, D. C. Montgomery, and C. M. Anderson-Cook:** *Response surface methodology: process and product optimization using designed experiments*. John Wiley & Sons, 2016

[9] **J. Zolgharnein, A. Shahmoradi, and J. B. Ghasemi:** *Comparative study of Box–Behnken, central composite, and Doehlert matrix for multivariate optimization of Pb (II) adsorption onto Robinia tree leaves*, *J. Chemom.*, vol. 27, no. 1–2, pp. 12–20, 2013

[10] **S. L. C. Ferreira *et al.*:** *Statistical designs and response surface techniques for the optimization of chromatographic systems*, *J. Chromatogr. A*, vol. 1158, no. 1–2, pp. 2–14, 2007

Journal of Energy Technology

JET Volume 12 (2019) p.p. 53-61
Issue 3, November 2019
Type of article 1.04
www.fe.um.si/en/jet.html

ELECTRIC AND MAGNETIC FIELD MEASUREMENTS FOR HIGH VOLTAGE TRANSMISSION LINES: THE CASE OF TURKEY

MERITVE ELEKTRIČNEGA IN MAGNETNEGA POLJA NA VISOKONAPETOSTNIH PRENOSNIH VODIH: NA PRIMERU TURČIJE

Mehmet Zeki Çelik[1,✉], Mehmet Murat Ispirli[2], Yusuf Öner[3], Bülent Oral[2]

Keywords: Electric field, ELF, Electromagnetic filed, ICNIRP, Magnetic field

Abstract

A power system is a facility that creates low-frequency electromagnetic fields (EMF) with its high-voltage level and high electric current capacity. In this respect, these electromagnetic fields need to be significantly evaluated from the aspects of both those who are exposed to the fields due to the structure of the facility during their daily lives and those who are exposed to the fields due to their occupation. In this study, the transmission lines and substations in the power system of Turkey are evaluated on account of electric and magnetic field measurements. Firstly, the people living in general public zones near the transmission line or substation were examined. In another part of the study, measurements were made in the occupational exposure of the staff in the energy zone. The results obtained from measurements are compared with the limit values provided by the International Commission on

✉ Corresponding author: Mehmet Zeki Çelik, Tel.: +90 505 747 9016, Mailing address: Turkish Electricity Transmission Corporation, Live Line Maintenance Engineering of Head, 34762, Istanbul, Turkey., E-mail address: mzekicelik@teias.gov.tr

[1] Turkish Electricity Transmission Corporation, Live Line Maintenance Engineering of Head, 34762, Istanbul, Turkey.

[2] Marmara University, Department of Electrical and Electronics Engineering, 34722, Istanbul, Turkey.

[3] Pamukkale Univesity, Department of Electrical and Electronics Engineering, 20070, Denizli, Turkey.

Non-Ionizing Radiation Protection (ICNIRP). The measurements were performed by NARDA EFA-300 electromagnetic field measurement. The closest point to the ground was determined as the reference point for the measurements performed on transmission lines. The results for different distances were obtained by performing measurements following those reference points with fixed distances.

Povzetek

Elektroenergetski sistem s svojo visokonapetostno stopnjo in visoko električno zmogljivostjo v okolju ustvarja nizkofrekvenčna elektromagnetna polja (EMF), ki jih je potrebno natančno ovrednotiti tako z vidika tistih, ki so izpostavljeni zaradi same strukture elektroenergetskega sistema v svojem vsakdanjem življenju, kot tistih, ki so poklicno izpostavljeni. V tej raziskavi so z vidika električnega in elektromagnetnega polja na podlagi meritev ovrednoteni daljnovodi in podpostaje v elektroenergetskem sistemu Turčije. V prvem delu raziskave so bile pregledane osebe, ki živijo v splošnih javnih conah v bližini daljnovoda ali podpostaj. V drugem delu so bile izvedene meritve pri poklicni izpostavljenosti osebja v energetskem območju, sami rezultati pa so primerjani z mejnimi vrednostmi, ki jih je zagotovila Mednarodna komisija za zaščito pred neionizirnimi sevanji (ICNIRP). Same meritve so bile izvedene z uporabo merilnika NARDA EFA-300, pri katerih je bila najbližja točka tal določena kot referenčna točka za meritve na daljnovodih. Rezultati za različne razdalje so dobljeni z izvajanjem meritev po referenčnih točkah s fiksno razdaljo.

1 INTRODUCTION

Power lines and electric appliances have separate electric and magnetic fields around them when current flows through them; specifically, these are not coupled electric and magnetic fields. The measurement of the electromagnetic fields that occur around the surroundings of transmission lines is performed via quantitative and analytical methods; the use of these methods began in the 1960s. The electricity current on the high-voltage transmission lines created low-frequency electromagnetic-fields on the environment. Much research has been carried out to investigate health hazards in connection with exposure to electric and magnetic fields from high voltage power lines. Reviews of the available data on the biological effects of exposure to these fields do not allow any definite conclusion concerning the health risk for the general population or for occupationally exposed workers. Concern that magnetic fields (MF) from power lines, commonly referred to as either “electromagnetic fields (EMF)" or "extremely low frequency (ELF) fields" may cause childhood leukaemia has continued to be expressed by some for many years, *[1-4]*.

Studies from the 1970s showed an increase that was statistically significant in childhood leukaemia for children living near power lines. Of the many additional studies since then, about half show small correlations with proximity to power lines and/or weak magnetic fields, and about half do not, *[5]*.

However, the possibility that there may be a cause and effect for long-term exposure to low levels of low-frequency electromagnetic fields has led to the classification by the International Agency for Research on Cancer (IARC), an agency of the World Health Organization (WHO), as a possible cause of cancer. However, this classification has not been included in the International Committee on Electromagnetic Safety or ICNIRP reference levels because of conflicting results and a lack of physical mechanisms by which weak magnetic fields could be expected to modify

biological systems. The IARC has published an extensive review of the research epidemiological and laboratory research used in its determination concerning cancer; the WHO previously published a similar monograph concerning low-frequency field effects and various diseases, including cancer, *[2, 5]*. The WHO/International Agency for Research on Cancer (IARC) has classified radiofrequency electromagnetic fields as possibly carcinogenic to humans (Group 2B), *[6]*. It is known that the electromagnetic field decreases as the distance from the source that generates the electric and magnetic fields increases.

The continuous increase in the demand for electrical energy, which has an essential place in daily life, reveals the necessity of a more reliable and quality energy concept. Technological criteria in the transmission of electrical energy must be taken into account. In order to operate safely and uninterruptedly, which is the measure of the quality of an electrical transmission system, in addition to the use of some technological developments, it is necessary to consider the electric and magnetic field parameters in the design and operation of the system. Considering the great number of high voltage equipment in the energy transmission systems and the effects of the field parameters generated by this equipment, it is necessary to investigate how are affected the field parameters in which the staff in the energy zone work and the people close to the energy zone live. The exposed electric and field electromagnetic values are given in Table 1 in the power transmission/distribution line for different voltages, *[7]*.

Table 1: *The samples values of electric and magnetic fields in overhead transmission lines at 50 Hz for different voltage levels*

The voltage level of the lines	Electric Field(V/m)			Magnetic Field (μT)		
	under the line	30 m away from axial	100 m away from axial	under the line	30 m away from axial	100 m away from axial
400 kV	5000	2000	200	30	12	1.2
225 kV	3000	400	40	20	3	0.3
90 kV	1000	100	10	10	1	0.1
20 kV	250	10	Negligible	6	0.2	Negligible
230 V	9	0,3	Negligible	0,4	Negligible	Negligible

Because taking into account electrical and magnetic field problems will be increased, high voltage systems should be examined according to the predefined and standardized field parameter sizes at the establishment and design stage.

In this context, the effective values of the magnetic and electric fields were measured in substation and power transmission lines. With these measurements, it was determined to what extent the staff in the energy area were exposed to these areas. Electromagnetic field exposure values were compared with similar studies and standards. In Turkey, as a result of these measurements are made to assessment about transmission system and substation and some suggestions.

2 CASE STUDY

2.1 Material and Methods

In Tables 2 and 3, the reference levels of occupational exposure and the general public for electric and magnetic fields are given. The reference levels assume that the human body is exposed to a homogeneous field and associated with the spatial extension, *[4]*.

Table 2: *Reference levels for occupational exposure to time-varying electric and magnetic fields (unperturbed rms values).*

Frequency range	Electric field strength E (kV/m)	Magnetic field strength H (A/m)	Magnetic flux density B (T)
1 Hz-8 Hz	20	$1{,}63\times10^{5}/^{2}$	$0{,}2/f^{2}$
8 Hz-25 Hz	20	$2\times10^{4}/f$	$2{,}5\times10^{-2}/f$
25 Hz-300 Hz	$5\times10^{2}/f$	8×10^{2}	1×10^{-3}
300 Hz-3kHz	$5\times10^{2}/f$	$2{,}4\times10^{5}/f^{2}$	$0{,}3/f$
3kHz-10 MHz	$1{,}7\text{x}10^{-1}$	80	1×10^{-4}

Table 3: *Reference levels for general public exposure to time-varying electric and magnetic fields (unperturbed rms values).*

Frequency range	Electric field strength E (kV/m)	Magnetic field strength H (A/m)	Magnetic flux density B (T)
1 Hz-8 Hz	5	$3{,}2\times10^{4}/f^{2}$	$4\times10^{-2}\text{m}/f^{2}$
8 Hz-25 Hz	5	$4\times10^{3}/f$	$5\times10^{-3}/f$
25 Hz-50 Hz	5	$1{,}6\times10^{2}$	2×10^{-4}
50 Hz–400 Hz	$2{,}5\times10^{2}/f$	$1{,}6\times10^{2}$	2×10^{-4}
400 Hz–3 kHz	$2{,}5\times10^{2}/f$	$6{,}4\times10^{4}/f$	$8\times10^{-2}/f$
3 kHz–10 MHz	$8{,}3\times10^{-2}$	21	$2{,}7\times10^{-5}$

The International Commission on Non-ionizing Radiation Protection (ICNIRP) has established guidelines for the protection of people exposed to electric and magnetic fields in the low-frequency range of electromagnetic fields. The low-frequency range of ICNIRP guides ranges from 1 Hz to 100 kHz.

ICNIRP guidelines above 100 kHz are within the protection range of 100 kHz to about 10 MHz. However, depending on the conditions of exposure to low-frequency effects on the nervous system, high-frequency effects should also be considered. Therefore, ICNIRP guidelines have been extended from 1Hz to 10 MHz to cover the effects of the nervous system.

The main purpose of ICNIRP is to provide guidelines for protection against all adverse health effects of electromagnetic fields and to limit exposure to electric and magnetic fields (EMF). Studies on both the direct and indirect effects of electric and magnetic fields are given by ICNIRP. Electromagnetic effects are caused by direct interaction of fields with the body; indirect effects include interactions with a conductive object when the electrical potential of the object is different from that of the body. The results of laboratory and epidemiological studies and reference levels for the assessment of hazard criteria for exposure to electric and magnetic

fields are discussed. Furthermore, the values stated in the ICNIRP apply to both those working under energy and those exposed to the public, *[8]*.

The measurements were made in a substation and transmission line for magnetic and electric field measurements. The devices for electrical and magnetic field measurements are placed in the working area at the height of 2 m from the ground. The maximum approach distances were determined in the measurements in the energy zone. Narda EFA-300 magnetic field and electric field measurement device shown in Fig.1 was used.

Figure 1: *The instrument used in the measurement*

Cross-sections of conductors and the approach distance information on the pole in electromagnetic investigations carried out on the energy transmission line measured as:

- The phase conductor heights from the ground at the measuring point: 16.89 m–17.04 m–16.47 m
- The protection conductor height from the ground: 26.13 m
- Conductor cross-section: 2×954 MCM

In this study, the limit values for extra-low frequency (ELF) electric field strength and magnetic induction by ICNIRP are considered.

2.2 Results and Discussion

The magnetic field on the power transmission line and the situated zero meter point specified in the electric field measurements are the maximum deflection point of the transmission line. “+60 m” and “-60 m” values are taken as the base 60 meters in front of and back of the maximum deflection point of the magnetic field and measured according to these distances. These magnetic and electric field measurements are shown on the graph in Fig. 2 and Fig. 3.

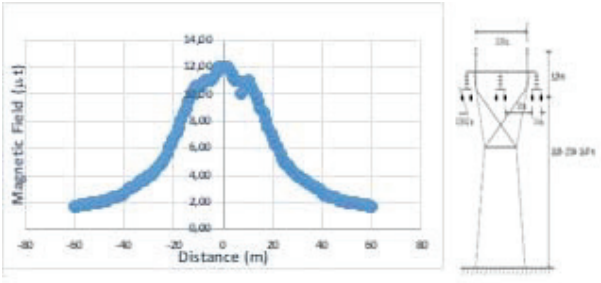

Figure 2: *The measured magnetic field for a transmission line with 400 kV for different distances*

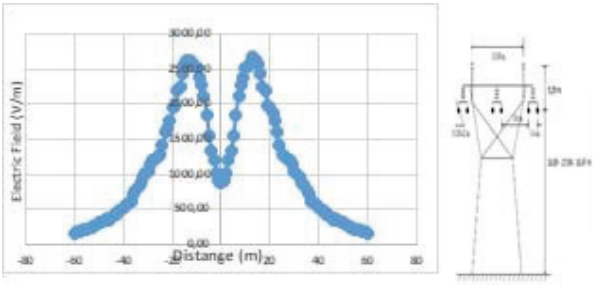

Figure 3: *The measured electric field for a transmission line with 400 kV for different distances*

After examining the transmission lines, the electromagnetic field measurements of the secondary side of 400 kV/154 kV transformer performed at Feeder 1 and Feeder 2 in the substation shown in Fig.4 measured as:

At Feeder 1:

- Current during measurement (A): A phase 334 A / B phase 338 A / C phase 330 A
- Voltage during measurement (kV): A-B phase 157.2 kV / B-C phase 156.2 kV / C-A phase 156 kV
- Conductor Distances: A phase 9.81 m / B phase 9.81 m / C phase 9.81 m
- Conductor cross-section: 954 MCM

At Feeder 2 :

- Current during measurement (A): A phase 334 A / B phase 326 A / C phase 328 A
- Voltage during measurement (kV): A-B phase 158 kV / B-C phase 156.6 kV / C-A phase 156.3 kV
- Conductor Distances: A phase 9.81 m / B phase 9.81 m / C phase 9.81 m

Figure 4: *The 400/154 kV substation in field measurements*

The situated zero meter point indicated in the magnetic and electric field measurements at the substation is the midpoint of Feeder 1 and Feeder 2. "+41 m" and "-41 m" values are taken as the basis of 41 meters right and left from the midpoint of Feeder 1 and Feeder 2. These magnetic and electric field measurements are shown on the graph in Fig. 5 and Fig. 6.

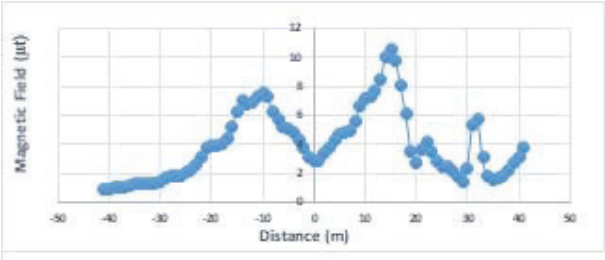

Figure 5: *The measured magnetic field for a substation with 154 kV for different distances*

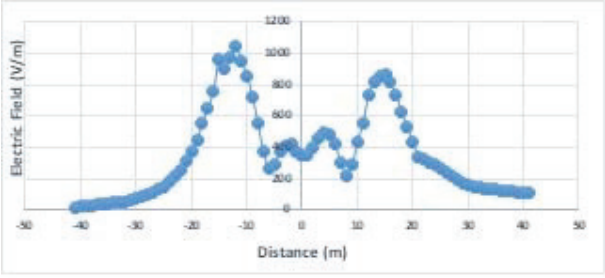

Figure 6: *The measured electric field for a substation with 154 kV for different distances*

3 CONCLUSION

Methods that reduce the effects of electric and magnetic fields are important for the health of both employees and people in public areas.

In this study, firstly, the people living in general public zones near the transmission line or substation are examined. In another part of the study, measurements were made in occupational exposure of the staff in the energy zone. Expanding these measurements will provide important data for both transmission lines and substation design.

In addition, the methods of reducing the electromagnetic effects in terms of the general public zone will raise the awareness of the people living nearby and will contribute to the spread of health measures.

The data obtained as a result of electromagnetic measurements will provide the necessary information about occupational diseases for the staff. Therefore, the investigation of electromagnetic effects on occupational safety and human health will contribute positively to reducing occupational diseases.

ELF in high voltage lines is important for people who are exposed to both occupational and public areas. Employees and the public should be informed about this issue.

The transmission system should be designed in line with the distances obtained during the measurements. The results of this study are below the measured values when compared with the relevant ICNIRP reference values.

As a result of the measurements, it is seen that both the people working under the voltage and the people living in the general public zones are exposed to the effects of the electric and magnetic fields.

References

[1] **F. Gamberale, O. Anshelm Olson, P. Eneroth, T. Lindh, A. Wennberg:** *Acute effects of ELF electromagnetic fields: a field study of linesmen working with 400 kV power lines*, British Journal of Industrial Medicine, Vol. 46, p.p. 729 – 737, 1989

[2] **P.A. Kokate, A.K. Mishra, S.K. Lokhande, G.L. Bodhe:** *Extremely Low-Frequency Electromagnetic Field (ELF-EMF) and childhood leukemia near transmission lines: a review*, Advanced Electromagnetics, Vol. 5, Iss. 1, p.p. 30 – 40, 2016

[3] **M. Repacholi:** *Concern that "EMF" magnetic fields from power lines cause cancer*, Science of the Total Environment, Vol. 426, p. p. 454 – 458, 2012

[4] **UK Childhood Cancer Study Investigators:** *Exposure to power-frequency magnetic fields and the risk of childhood cancer*, The Lancet, Vol. 354, Iss. 9194, p.p. 1925 – 1931, 1999

[5] **F. Barnes, B. Greenebaum:** *Some Effects of Weak Magnetic Fields on Biological Systems*, IEEE Power Electronics Magazine, Vol. 3, Iss. 1, p.p. 60 – 68, 2016

[6] **The International Agency for Research on Cancer (IARC):** [Online], Available: https://monographs.iarc.fr/list-of-classifications. Accessed 10 May 2019

[7] **Gestionnaire de Réseau de Transport d'Electricité**: *Les champs électromagnétiques de très basse fréquence*, 2005

[8] **International Commission on Non-Ionizing Radiation Protection**: *Guidelines for limiting exposure to time-varying electric and magnetic fields (1 Hz to 100 kHz),* Health Physics Society, Vol. 99, Iss. 6, p.p. 818 – 836, 2010

Nomenclature

(Symbols)	(Symbol meaning)
A	Ampere
B	Magnetic flux density
E	Electric field strength
f	Frequency
H	Magnetic field strength
Hz	Hertz
m	Meter
MCM	Micro Circular Mil
T	Tesla
V	Volt

JET Journal of Energy Technology

Author instructions

www.fe.um.si/en/jet.html

MAIN TITLE OF THE PAPER
SLOVENIAN TITLE

*Author[1], Author [2], Corresponding author*ℜ

Keywords: (Up to 10 keywords)

Abstract

Abstract should be up to 500 words long, with no pictures, photos, equations, tables, only text.

Povzetek

(Abstract in Slovenian language)

Submission of Manuscripts: All manuscripts must be submitted in English by e-mail to the editorial office at jet@um.si to ensure fast processing. Instructions for authors are also available online at http://www.fe.um.si/en/jet/author-instructions.html.

Preparation of manuscripts: Manuscripts must be typed in English in prescribed journal form (MS Word editor). A MS Word template is available at the Journal Home page.

A title page consists of the main title in the English and Slovenian language; the author(s) name(s) as well as the address, affiliation, E-mail address, telephone and fax numbers of author(s). Corresponding author must be indicated.

Main title: should be centred and written with capital letters (ARIAL bold 18 pt), in first paragraph in English language, in second paragraph in Slovenian language.

Key words: A list of 3 up to 6 key words is essential for indexing purposes. (CALIBRI 10pt)

Abstract: Abstract should be up to 500 words long, with no pictures, photos, equations, tables, - text only.

Povzetek: - Abstract in Slovenian language.

Main text should be structured logically in chapters, sections and sub-sections. Type of letters is Calibri, 10pt, full justified.

ℜ Corresponding author: Title, Name and Surname, Organisation, Department, Address, Tel.: +XXX x xxx xxx, E-mail address: x.x@xxx.xx

[1] Organisation, Department, Address

[2] Organisation, Department, Address

Units and abbreviations: Required are SI units. Abbreviations must be given in text when first mentioned.

Proofreading: The proof will be send by e-mail to the corresponding author in MS Word's Track changes function. Corresponding author is required to make their proof corrections with accepting or rejecting the tracked changes in document and answer all open comments of proof reader. The corresponding author is responsible to introduce corrections of data in the paper. The Editors are not responsible for damage or loss of submitted text. Contributors are advised to keep copies of their texts, illustrations and all other materials.

The statements, opinions and data contained in this publication are solely those of the individual authors and not of the publisher and the Editors. Neither the publisher nor the Editors can accept any legal responsibility for errors that could appear during the process.

Copyright: Submissions of a publication article implies transfer of the copyright from the author(s) to the publisher upon acceptance of the paper. Accepted papers become the permanent property of "Journal of Energy Technology". All articles published in this journal are protected by copyright, which covers the exclusive rights to reproduce and distribute the article as well as all translation rights. No material can be published without written permission of the publisher.

Chapter examples:

1 MAIN CHAPTER

(Arial bold, 12pt, after paragraph 6pt space)

1.1 Section

(Arial bold, 11pt, after paragraph 6pt space)

1.1.1 Sub-section

(Arial bold, 10pt, after paragraph 6pt space)

Example of Equation (lined 2 cm from left margin, equation number in normal brackets (section. equation number), lined right margin, paragraph space 6pt before in after line):

Equation (1.1)

Tables should have a legend that includes the title of the table at the top of the table. Each table should be cited in the text.

Table legend example:

Table 1: *Name of the table (centred, on top of the table)*

Figures and images should be labelled sequentially numbered (Arabic numbers) and cited in the text – Fig.1 or Figure 1. The legend should be below the image, picture, photo or drawing.

Figure legend example:

Figure 1: *Name of the figure (centred, on bottom of figure, photo, or drawing)*

References

[1] **N. Surname:** *Title,* Journal Title, Vol., Iss., p.p., Year of Publication

[2] **N. Surname:** *Title,* Publisher, Year of Publication

[3] **N. Surname:** *Title* [online], Publisher or Journal Title, Vol., Iss., p.p., Year of Publication. Available: website (date accessed)

Examples:

[1] **J. Usenik**: *Mathematical model of the power supply system control*, Journal of Energy Technology, Vol. 2, Iss. 3, p.p. 29 – 46, 2009

[2] **J. J. DiStefano, A.R. Stubberud, I. J. Williams**: *Theory and Problems of Feedback and Control Systems*, McGraw-Hill Book Company, 1987

[3] **T. Žagar, L. Kegel:** *Preparation of National programme for SF and RW management taking into account the possible future evolution of ERDO* [online], Journal of Energy Technology, Vol. 9, Iss. 1, p.p. 39 – 50, 2016. Available: http://www.fe.um.si/images/jet /Volume 9_Issue1/03-JET_marec_2016-PREPARATION_OF_NATIONAL.pdf (7. 10. 2016)

Example of reference-1 citation: In text *[1],* text continue.

Nomenclature

(Symbols)	(Symbol meaning)
t	time

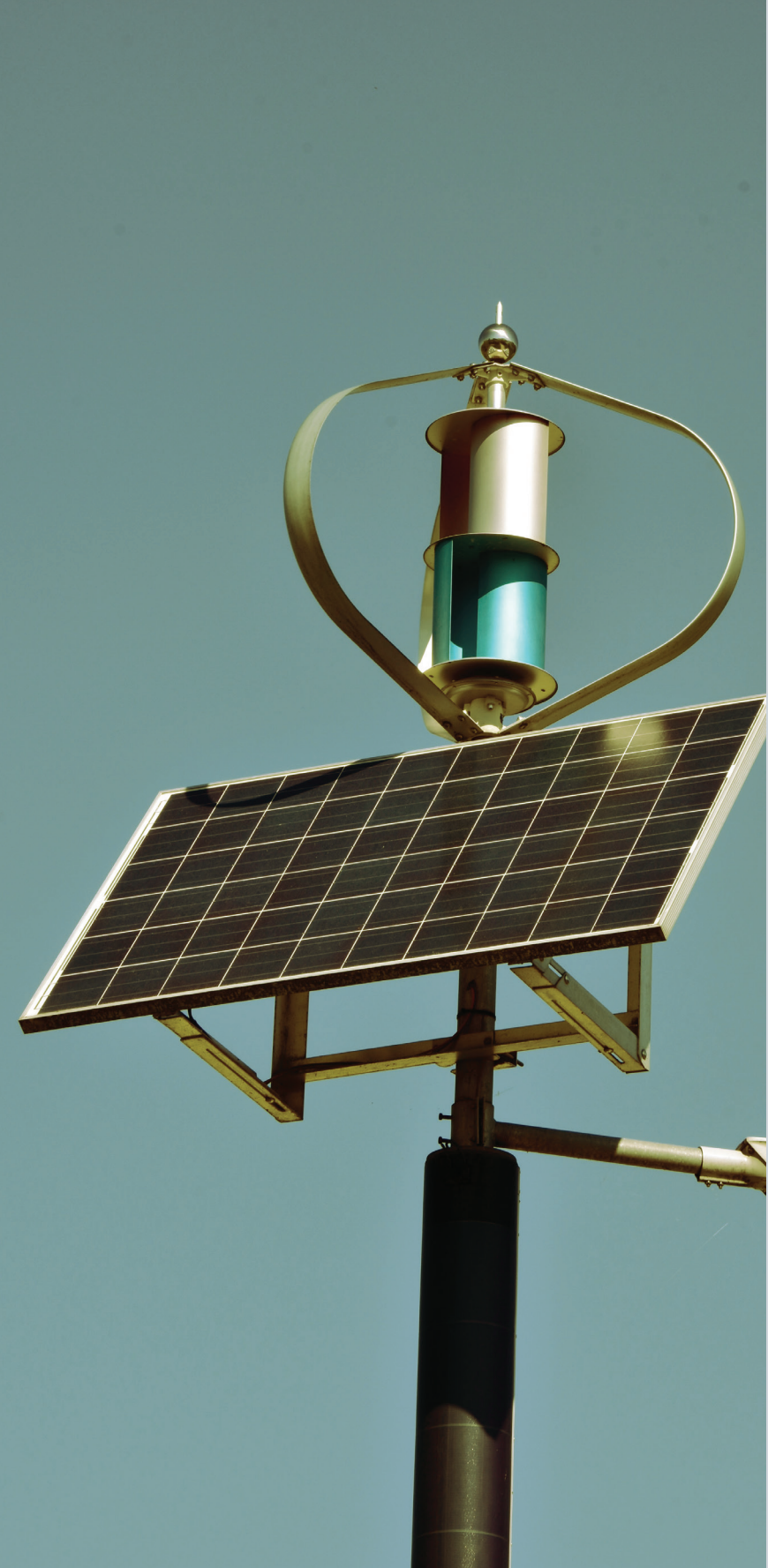

JET

JET I Journal of Energy Technology I Vol. 12, Issue 3, November 2019 I University of Maribor, Faculty of Energy Technology

ISSN 1855-5748

9 771855 574008